2017-06-01

Flexible Micro-N-Line Probe and Apparatus to Characterize Electronic Conductivity of Li-ion Battery Electrode Films

Derek Van Clement
Brigham Young University

BYU ScholarsArchive Citation

Clement, Derek Van, "Flexible Micro-N-Line Probe and Apparatus to Characterize Electronic Conductivity of Li-ion Battery Electrode Films" (2017). *All Theses and Dissertations*. 6550.
https://scholarsarchive.byu.edu/etd/6550

Flexible Micro-N-Line Probe and Apparatus to Characterize Electronic Conductivity of Li-ion Battery Electrode Films

Derek Van Clement

A thesis submitted to the faculty of
Brigham Young University
in partial fulfillment of the requirements for the degree of

Master of Science

Brian A. Mazzeo, Chair
Dean R. Wheeler
Aaron R. Hawkins

Department of Electrical and Computer Engineering

Brigham Young University

ABSTRACT

Flexible Micro-N-Line Probe and Apparatus to Characterize Electronic Conductivity of Li-ion Battery Electrode Films

Derek Van Clement
Department of Electrical and Computer Engineering, BYU
Master of Science

A key metric that affects Li-ion battery cell performance is the electronic conductivity of the electrode films. Previous research has found that the conductivity of electrodes is not homogeneous throughout the entirety of the deposited film area. To further characterize the non-homogeneity of the conductivity of electrode films, a micro-N-line probe (μNLP) and a micro-flex-line probe (μFLP) were developed to take micro-scale conductivity measurements of thin-film battery electrodes in a non-destructive manner. These devices have been validated by comparing test results to those of it's predecessor, the micro-four-line probe (μ4LP), on various commercial-quality Li-ion battery electrodes. Results show that there is significant variation in conductivity on a millimeter and even micrometer length scale throughout the electrode film. Compared to the μ4LP, the μNLP and μFLP perform six times as many measurement configurations made on contact with the electrode, while providing a more robust design. Design improvements on the μ4LP in order to fabricate the μFLP are the main focus of this thesis. Researchers and manufacturers can use this probe to identify heterogeneity in their electrodes during the fabrication process, which will lead to the development of better batteries.

Keywords: Li-ion Battery, Conductivity, Electrode, Flexible

ACKNOWLEDGMENTS

I would like to acknowledge my parents, Lisa and Jay Clement, for always giving me encouragement through rough times and starting me on the path towards engineering. I would also like to thank my wife Kimberlee, for staying by my side and supporting me through this process. I would also like to acknowledge my advisers, Dr. Mazzeo and Dr. Wheeler, as well as my co-workers, John Vogel, Andrew Cutler, and Emilee Hardy for helping me to achieve a Master of Science Degree in Electrical and Computer Engineering.

CONTENTS

LIST OF TABLES

LIST OF FIGURES

NOMENCLATURE

I	Current
R	Resistance
V	Voltage
σ	Electronic Conductivity

CHAPTER 1. INTRODUCTION

1.1 Motivation

Rechargeable batteries, also known as secondary batteries, are an important component of modern day life. They are critical elements used to power everything from toys to cars. Being able to recharge a device while resting or on the go is expected for almost any electronic device purchased. One of the most popular chemistries for secondary batteries is lithium-ion (Li-ion). Li-ion batteries are the current standard for powering portable electronics such as smart-phones, tablets, laptops, and many other recreational electronics. Because of this, the global Li-ion battery market was a \$29.68 bn industry in 2015 and is projected to rise to \$77.42 bn by the year 2024 [1]. According to Statista, it is predicted that consumer electronics and electric vehicles will account for more than 54% of the global Li-ion battery market in 2020 [2]. This prediction can be easily achieved by the rise of smart-phone technology and advancements that Tesla and other manufacturers are making in their electric cars.

There are a few different cell designs for Li-ion batteries. Cylindrical Li-ion batteries are the most common thin-film cell design for consumer secondary batteries today. They are overwhelmingly used in the commercial battery world for powering electric vehicles. The most popular size for cylindrical cells is the 18650 cell, meaning the cell is 18 mm in diameter and 65 mm in length. Figure 1.1 shows how a typical cylindrical cell is composed. An anode and cathode are spirally wound with a separator layer between them that allows ions to flow in-between them to form the battery. The resulting “jellyroll” is then stored in a metal battery casing, allowing the positive and negative terminals to be accessed.

The cells have high discharge and recharge efficiencies, and strong durability over thousands of cycles. Depending on specific sub-chemistries of Li-ion technology, Table 1.1 shows typical values for thin-film Li-ion battery characteristics [3], [4]. Thin-film battery cells have high energy densities due to the film being rolled up on its self.

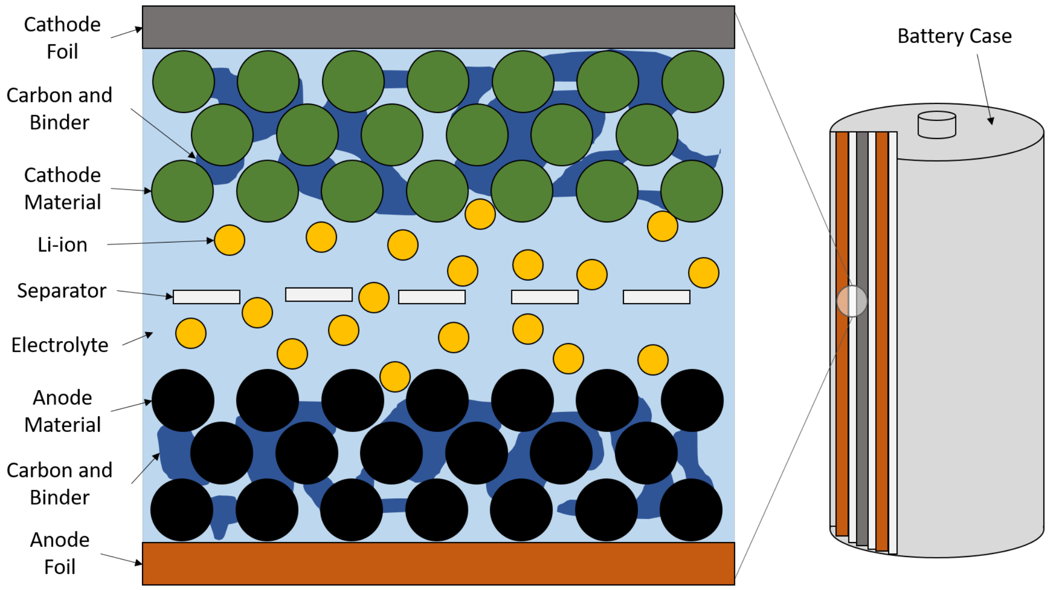

Figure 1.1: Basic structure of a thin-film Lithium-ion battery cell and orientation of the anode and cathode.

Table 1.1: Typical Range of Characteristics for Thin-Film, Lithium-ion Battery Electrodes.

Characteristic	**Typical Value**
Specific Energy	70–260 W·h/kg
Charge/Discharge Efficiency	80–90%
Cycle Durability	300–2000 cycles
Nominal Cell Voltage	2.4–3.8 V

A single Telsa Model S battery pack uses more than 7,000 18650 cells to power the vehicle. This is a large sum just for one car, but with almost 84,000 Tesla electric cars sold worldwide in 2016, this number increases to roughly 0.6 bn cylindrical cells used by Tesla Inc. in 2016 alone [5]. Not only are thin-film Li-ion batteries taking over the electric car industry, but they have already dominated the electronic hand-held device market, consisting mainly of mobile phones. There are more than 324 million documented Americans living in the United States and roughly two-thirds of them are adults [6]. According to the Pew Research Center, 64% of American adults now own a smart-phone, increasing from 58% in 2014 [7]. From this, it is estimated that roughly 162 million American adults own a smart-phone and purchase a new one about every 2 years. This number will only grow. Each one of these smart-phones is powered by a thin-film Li-ion battery pack identical in chemical make-up to the cylindrical Li-batteries, but different in design because of their thinner, rectangular packaging. It is clear that Li-ion batteries are an integral part of typical American life and the same can be said for nearly every other country on earth.

Due to the demand for high-quality secondary batteries, the improvement of Li-ion electrode films is a necessary focus for many research groups. One such group, which we do research for, is the Battery Materials Research (BMR) group funded by the Department of Energy. In order to further the technology that Li-ion batteries power, the battery technology itself must be furthered.

Failed attempts at integrating underdeveloped Li-ion battery technology can be seen in the Boeing 787 and Samsung Note 7 battery incidents that occurred in 2013 and 2016 respectively. In both instances the batteries experienced thermal runaway, resulting in fires [8], [9]. This endangered many individuals. For these two cases, the resulting battery failures were extreme, and affected the battery in ways clearly seen by the user. Failures like these aren't typical. However, the presence of microscopic manufacturing defects in the thin film electrode is typical and hinders the lifetime and energy density in ways not initially detectable to the user of the battery. This thesis addresses these defects and characterizes them through a method developed to measure them.

A key metric in battery performance is the volume-averaged (effective or bulk) electronic conductivity of electrode film [10]. It is common to see conductivity in different thin-film electrodes range from 10 mS/cm to 1500 mS/cm, depending on the type of active material present, amount of carbon and binder used and concentration of lithium present in the film. The electronic conductivity of a material is a measure of how well electrons flow through the electrode medium from one point to another. When electron flow (current) is hindered, this means conductivity decreases. Equation 1.1 shows that conductivity is inversely proportional to the measurement of a materials resistance for a given geometry, where σ is conductivity, R is resistance, A_c is the cross-sectional area of the material, and ℓ is the length of the material. High conductivity means current flows easily through the material, and low conductivity means current flow is inhibited.

$$\sigma = \frac{\ell}{\mathrm{RA}_c} \tag{1.1}$$

From the use of ℓ and A_c in Equation 1.1, it is seen that electrical conductivity is dependant upon the geometric structure of the material arrangement within the thin film. An example of the final micro-structure of an electrode film is seen in the inset scanning-electron microscope (SEM) image in the top left of Figure 1.2. The non-uniform distribution of pores, active material and carbon binder is an end result of the commercial fabrication processes used to manufacture thin-film electrodes. The first step in a typical fabrication process is to mix a slurry that contains active material, carbon additive, binder, and a carrier solvent. The slurry is then spread onto a thin metal foil, typically by using a blade to control the thickness of the coating. This process is shown in Figure 1.2.

After the slurry is spread onto the current collector, it is dried, calendered, and cut to the necessary dimensions needed for the battery. The drying process does not guarantee a uniform distribution of carbon and active material when the solvent is driven out during the drying stage. A non-uniform spatial distribution of pores forms. This non-uniformity can be seen in the SEM image in the top left of Figure 1.2.

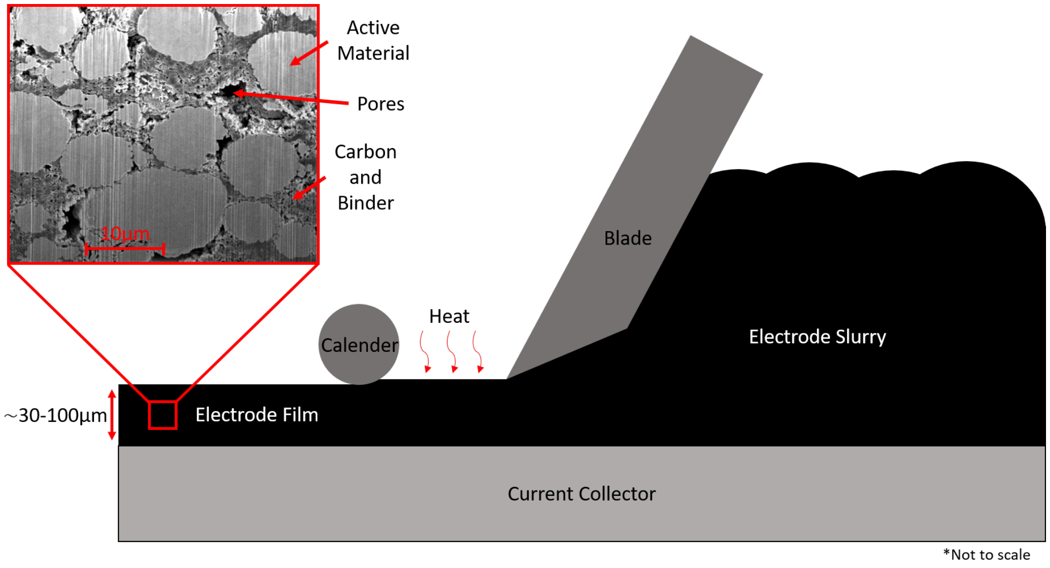

Figure 1.2: Electrode slurry coated onto a current collector by use of a blade to control the resulting height. The inset scanning-electron microscope image shows how the slurry forms a non-uniform distribution of carbon, active material, and pores after the drying stage.

These non-uniform distributions result in variable electronic conductivity on a micron-scale due to current favoring one path through the material more than another [11]. These favored sections in the material where current flows more easily are what we call “hot spots”. The opposite are called “cold spots”.

Hot spots in the battery film lead to under-performance of electrodes and even early battery failure due to uneven currents and potentials in the electrode. Current travels through the path of least resistance. If a few locations in the electrode favor a higher current flow, it wears the film out faster in those particular areas. As electrons travel from one location to another, over time they can slowly damage the medium that they travel through. This inhibits optimal usage of the active material.

While this variability in conductivity is a known characteristic of electrode films [12], steps need to be taken to successfully quantify it. This thesis introduces an improved method to test for micron-scale heterogeneity of conductivity in thin-film battery electrodes. Through this method of testing for spatial heterogeneity of conductivity, correlation between structure and conductivity can be explored to create higher quality thin-film electrodes to be used in batteries.

1.2 Literature Review

Many methods have been explored to make conductivity measurements of thin-film battery material. Prior research performed by Ramdon et al. [13] and Kerlau et al. [14] used current-sensing atomic force microscopy to calculate micro-scale conductivity readings of various surfaces. This method produces high spatial resolution in surface conductivity and allows for good imaging capabilities, but cannot probe the conductivity of the material below the surface particles. There is also large and varying contact resistance between the probe tip and and the surface that is difficult to estimate when using this method. Contact resistance is resistance that forms between the interface of two surfaces. It is a variable that must be properly accounted for in order to accurately estimate conductivity of the underlying material.

Multi-point probes hold an advantage in that they can theoretically eliminate the contact resistance caused by the probe and the surface using four-point theory. This is often used in semi-conductor processes, as was shown by Smits [15] in 1957. Perkins et al. [16] explored a micro-scale method for conductivity characterization by using a multi-point probe in ultra-high vacuum.

In that work, a variety of the possible contact configurations provide for a wide range of measurement spacing, but probe breakage due to pressure control complications made this method expensive and time-consuming.

Previous researchers in the BMR group built a micro-four-line probe (μ4LP) based off four-point theory [17]. This probe was able to measure variations in bulk conductivity in thin-film battery electrodes on a micron-scale using a non-destructive method [12]. This thesis introduces probes that improve upon the design of the μ4LP to more accurately measure spatial variations in conductivity.

1.3 Contributions

Personal contributions that I have made to this project include:

- Fabrication of newly developed probes
- Design and fabrication of a flexible probe
- Development of a novel mounting process of a flexible substrate onto a glass wafer
- Improvements to a previously created measurement apparatus
- Construction of a new, cost-effective, and portable measurement apparatus

1.4 Overview

The remainder of this thesis is organized into five chapters as follows: Chapter 2 provides a background to this project and the probes that are used to take conductivity measurements on thin-film battery electrodes. Chapter 3 introduces changes and improvements made to the μ4LP, and explains the necessary steps to fabricate the modified probes. Chapter 4 covers the two different measurement apparatuses used to take measurements with each probe. Chapter 5 discuses the test results and compares the data to past data acquired. Finally, Chapter 6 concludes this thesis with experimental conclusions, contributions to fields of study, and areas of future study in the project.

CHAPTER 2. BACKGROUND

2.1 Previous Work

Previous work from our BMR group was inspired by modified four-point theory. Four-point theory was first adapted into a 15 cm × 15 cm, four-line probe by Peterson and Wheeler [18]. The use of lines allows for good contact and avoids the possibility of puncturing the film and probing the current collector instead of the battery film, see Figure 2.1.

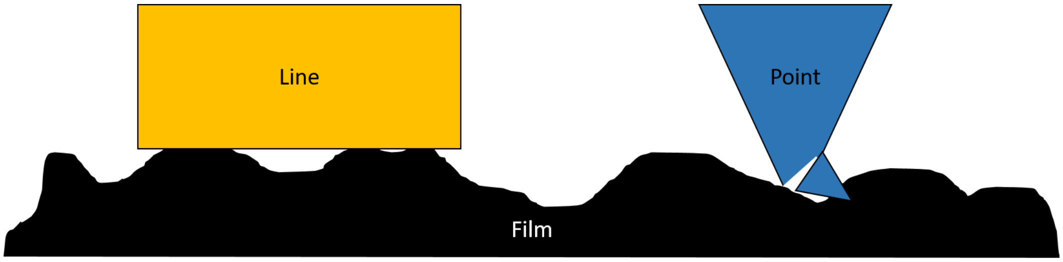

Figure 2.1: Schematic showing the difference between using a line to probe the electrode film versus using a point. Points are prone to breaking, due to the difficulty of controlling contact force.

Originally, measurements were taken with the macro (>1 mm) four-line probe by delaminating the electrode film from its current collector and pressing the four-line probe against it. This method provides an excellent way to calculate average of bulk conductivity by following Equation 2.1, where σ is conductivity, ℓ is the length of the sample, I is the current that passes through the sample, ΔV is the voltage difference of the two inner lines, and A_c is the cross-sectional area of the sample.

$$\sigma = \frac{\ell \mathrm{I}}{\Delta \mathrm{V} \mathrm{A}_c} \tag{2.1}$$

While this method worked well, it is destructive to the film to delaminate it from the current collector. Destructive testing is allowable from a research standpoint, but is not ideal for in-line testing by manufactures during the fabrication of battery electrodes. Figure 2.2 shows how the current collector was removed to eliminate shunt current, allowing for the measurement of the the electrode film alone.

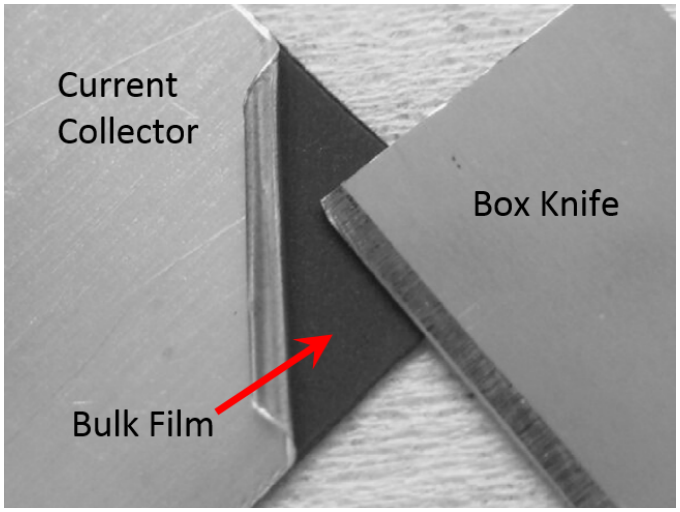

Figure 2.2: An example of delaminating the current collector from the electrode film, allowing for conductivity testing of the film. This process is destructive to the electrode.

It is difficult to measure bulk conductivity of electrodes due to the current collector acting as a shunt path for the current. This shunt path is shown in Figure 2.3, as the path of the current is shown to travel through the current collector as well as the electrode film. For this reason, the current collector was removed in the experiments. To solve not having to remove the current collector in order to perform conductivity measurements, Lanterman et al. [12] developed the μ4LP in order to take micro-scale (>1 μm and <1 mm) conductivity measurements. This probe is shown in Figure 2.4.

As shown in Figure 2.3, the μ4LP uses the two outside lines to pass current and the two inside lines to collect a voltage difference. The data collected is used to calculate the bulk conductivity of the sample by applying the mathematical model developed by Flygare et al. [17]. The model is modular in that it accounts for probe and sample geometry. It is important that the mathematical model is able to take varying values for the window dimensions because line geometries and spacing changed throughout the duration of the project in order to find working parameters.

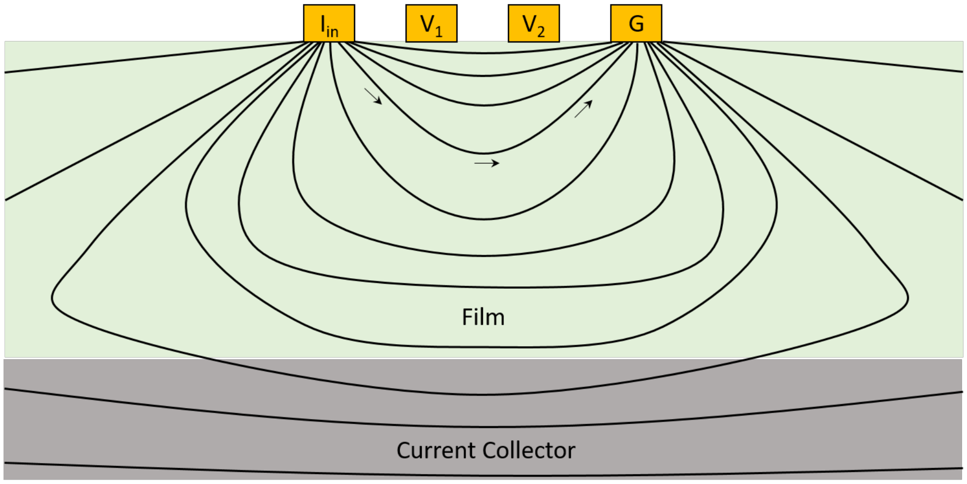

Figure 2.3: Schematic of how current travels through the electrode film and current collector.

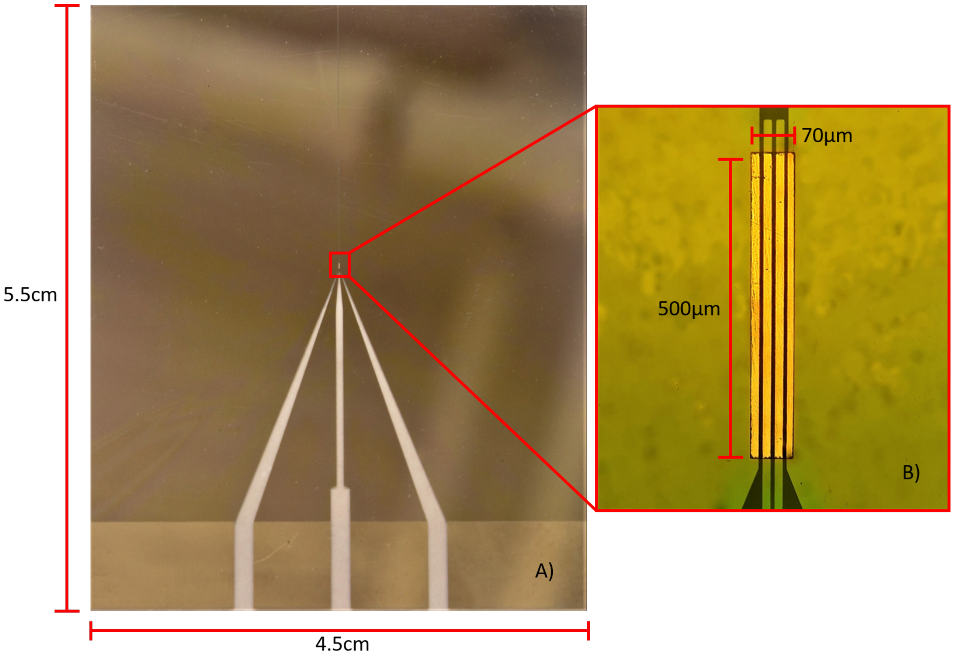

Figure 2.4: Picture and dimensions of a finished μ4LP (A) and its window (B) [12].

The spacing and width of the lines inside the window are determined by typical characteristics of Li-ion battery electrode films. The two film characteristics that determine the dimensions of the window are the film thicknesses (∼30–100 μm), and the surface roughness of the film (∼3–5 μm). The ranges of these two characteristics are determined by the active material's chemistry and particle size. The width of each line has to be such that it is able to make consistent contact with the electrode surface. The spacing of the lines has to be such that the volume measured consists of many particles and not just a few, so an appropriate average is calculated.

Through prior research, it was found that the distance between the two outer lines used to take a measurement should be approximately the same as the electrode film thickness [17]. When the window dimensions are as such, a minimal shunt current passing through the current collector is accounted for and calculated out of the final conductivity measurement for that sample location. By using the μ4LP in a grid-like pattern, conductivity maps are created to visually show hot and cold spots in the electrode film. Figure 2.5 shows one such map constructed from data sampled by a μ4LP [12]. It is a local conductivity plot of 16 different locations on cathode AC005 donated by Argonne National Laboratory for testing.

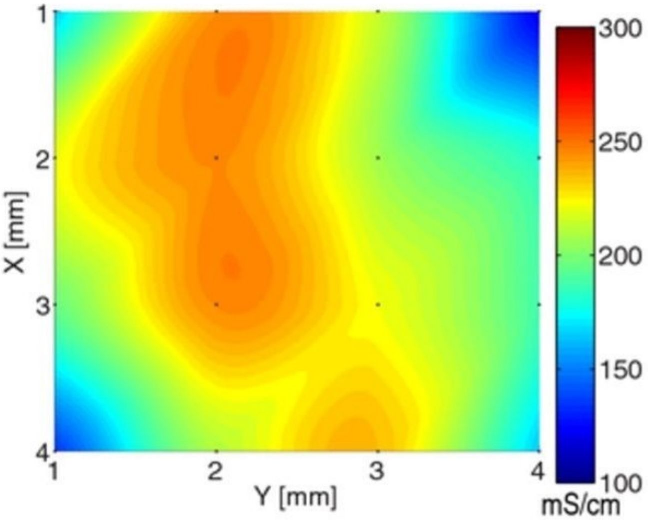

Figure 2.5: Local conductivity plot of 16 different locations on a 4mm × 4mm sample of the cathode AC005 distributed by Argonne National Laboratory. This figure was published by Lanterman et. al. [12].

2.2 Thesis Project

Previous research performed with the μ4LP has found that local conductivity of various thin-film electrodes can vary by up to an order of magnitude [12], creating hot and cold spots of conductivity in the film. This heterogeneity is found throughout the entire area of the film on a millimeter and even micrometer scale. While the μ4LP is functional, this thesis introduces the micro-N-line probe (μNLP) which has various improvements in design that enhance the robustness of the probe and increase measurement efficiency. In addition to the μNLP, this thesis introduces the micro-Flex-line probe (μFLP). This probe is based on the same design as the μNLP, except it is fabricated on a flexible substrate which adds diversity in functionality and improves durability in overall probe strength.

In this thesis, it is shown how my contributions to the BMR group advances the project by introducing a new and improved probe used for the testing of conductivity in thin-film battery electrodes. Various features have been added and changed in the design of the μ4LP and measurement apparatus in efforts to make the μNLP and μFLP ideal for measuring conductivity of thin-film electrodes:

- Instead of four lines, there are now N lines, where N represents the number of lines that could be present on the probe. In this thesis we will discuss our probe design that uses 6 lines.
- A comprehensive change has been wrought in the design of the contact window area, and measurement line geometry.
- To accommodate the changes in the μNLP, updates have been made to the measurement apparatus and software.
- A new measurement apparatus was developed and created to accommodate the μFLP.

These comprehensive changes in design and methodology translate to a more robust and modular probe. The probe, used in conjunction with the enhanced measurement apparatus, will be used for characterizing micro-scale bulk conductivity variation in thin-film battery electrodes.

CHAPTER 3. METHODOLOGY AND FABRICATION

3.1 Introduction

Many design changes, both macro and micro, have been made to the μ4LP in developing the μNLP and μFLP. The progression of the probe design can be briefly seen in Figure 3.1 as it transitions from the the μ4LP on the left to the μFLP on the right. This chapter of the thesis will address the fabrication of the μNLP and μFLP while also explaining the reasoning behind the changes made from the original μ4LP. The μNLP will be addressed first, then the μFLP. The purpose of this chapter is to outline the design improvements made to the μ4LP in order to introduce the μFLP, which is the main outcome of this project.

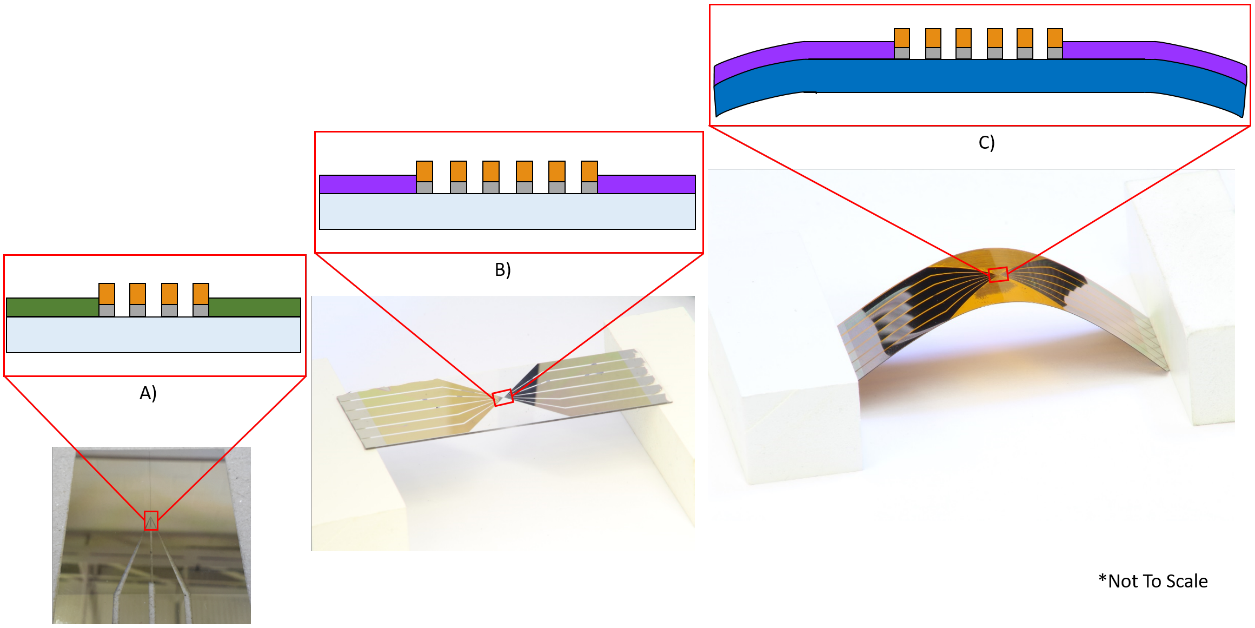

Figure 3.1: Progression of probe design from the μ4LP (A) to the μNLP (B) to the μFLP (C). A profile of the "window" for each of the probes is respectively blown-up above each.

3.2 Micro-N-Line Probe

3.2.1 Probe Design Improvements for Micro-N-Line Probe

To improve the performance of our probes, many different features of the μ4LP were changed and added to design and fabricate the μNLP. This section address these changes and why they are necessary to improving the performance of the probe.

Square Window

The window of the probe is possibly the most important feature on the device. It is where the probe makes contact with the electrode and where measurements are performed. The window is named as such because it is the rectangular area of the device that does not have a protective coating of SU-8, allowing the measurement lines to make contact with the electrode surface. Figure 3.2 shows a CAD rendering of the measurement window. It was found that non-destructive testing is possible, when the width of the probe window is on the same order as the thickness of the electrode film.

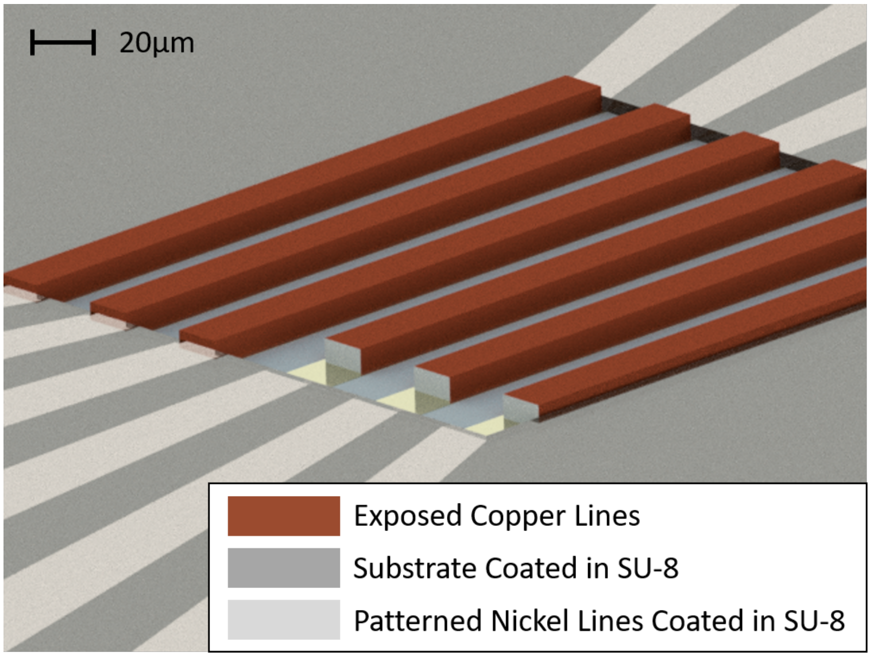

Figure 3.2: CAD rendering of a finished probe window. There is a section of the copper lines cut out to show how the lines protrude from the SU-8 to make contact with the electrode.

There is flexibility in the design of the window because a mathematical model takes into account the distribution of current for the probe in the geometry of the sample volume. Taking the mathematical model into account, each line of the μNLP is 20 μm × 250 μm, with 20 μm spacing between each line. This creates a semi-square window with a width of 220 μm and a length of 250 μm.

The decision to move towards a wider, square window as opposed to the rectangular window of the μ4LP was motivated by both ease of fabrication, and the intuitive nature of analyzing conductivity measurements on a square map. 20 μm wide lines are more robust during the fabrication process and snap off less often during testing compared to the 10 μm wide lines used in the μ4LP. Because of the 250 μm width of the window, more current passes through the current collector during testing. This is not ideal, but the model previously mentioned can account for this, while still allowing for characterization of conductivity on a micron-scale.

Six Measurement Lines

The μNLP has six lines compared to the four lines on the μ4LP. Having six lines does nothing to change the manner in which a measurement is taken, meaning that four-line probe theory still applies. When taking measurements, four lines are used to take types of measurements per contact with the electrode. These two measurements are shown in Figure 3.3. The top measurement seen is a tangential measurement, meaning a calculation of resistivity is made by passing current (I_{in}) from the input voltage source (V_{in}) to Ground (G). The bottom measurement is an orthogonal measurement, meaning a calculation is made by applying V_{in} to two lines and measuring I_{in} as it passes through the grounded current collector of the electrode. Each measurement configuration includes two lines used to measure the voltage difference between Voltage 1 (V_1) and Voltage 2 (V_2). Both the tangential and orthogonal measurements are necessary in calculating the bulk conductivity of the sampled volume.

The addition of two lines increases the number of measurements per contact that can be made with both the tangential and orthogonal configurations. From the six measurement lines, four can be chosen at a time for each measurement (three to measure I_{in}, V_1, and V_2, and one that acts as Ground). Knowing this, we can use Equation 3.1 to calculate that there are 360 different measurement permutations possible.

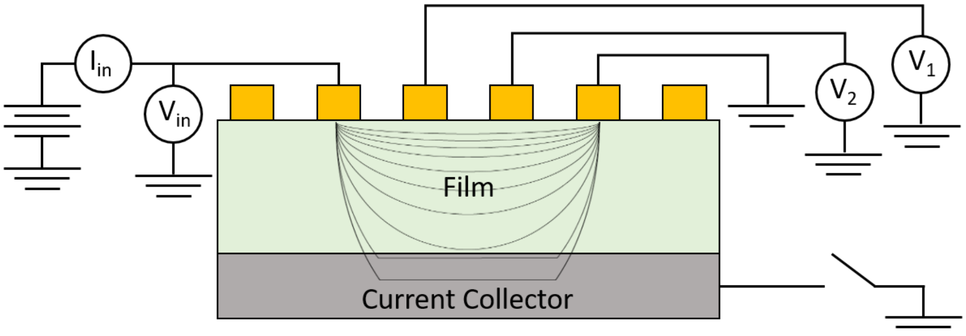

Tangential Measurement

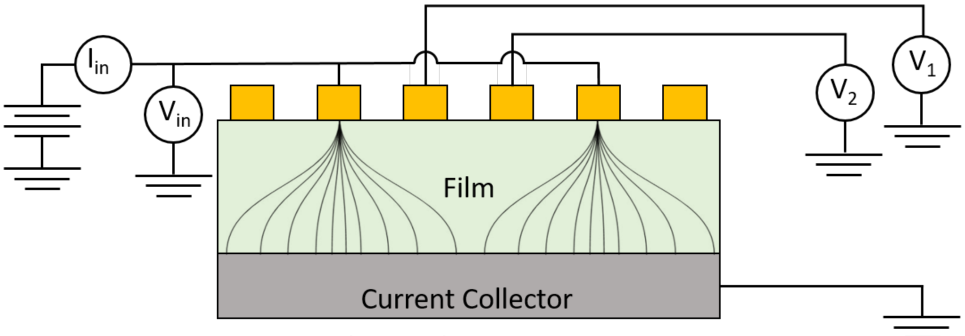

Orthogonal Measurement

Figure 3.3: Schematic of a tangential and orthogonal measurement setup using the μNLP on a thin film electrode. Current lines are shown to represent how the current flows through the electrode differently for both types of measurements.

$$P(6,4) = \frac{6!}{(6-4)!} = 360 \tag{3.1}$$

Only six of the 360 measurements are currently used for the purpose of measuring conductivity. Each of these six measurement for both the tangential and orthogonal configurations are represented in Figure 3.4. This figure shows the twelve different measurement configurations that are made with the μNLP on each contact with the electrode. The positively labeled measurement configurations are the measurements used to collect the data that was analyzed for this thesis. The negatively labeled configurations are collected as well to analyze how the measurements are effected when V_1 and V_2 are on the outside of the current path. Further analysis is needed to know if the negative measurement configurations provide any relevant data.

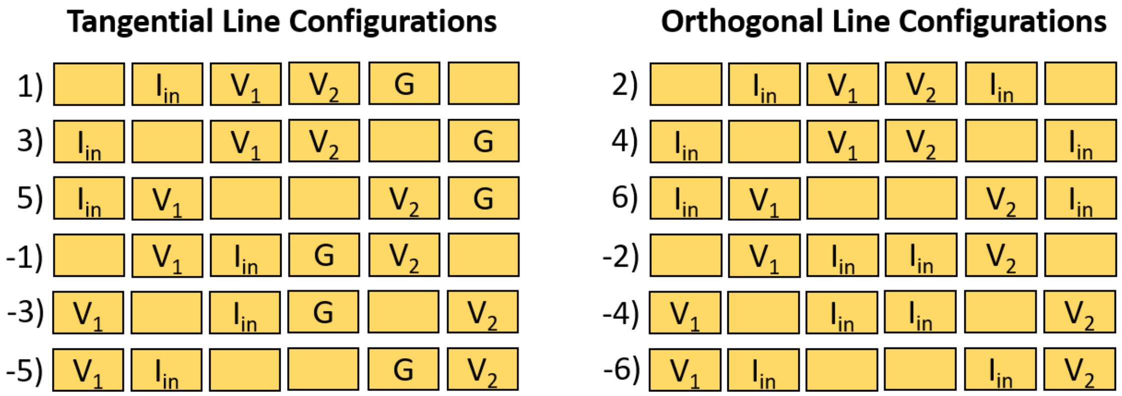

Tangential Line Configurations

1)		I_{in}	V_1	V_2	G	
3)	I_{in}		V_1	V_2		G
5)	I_{in}	V_1			V_2	G
-1)		V_1	I_{in}	G	V_2	
-3)	V_1		I_{in}	G		V_2
-5)	V_1	I_{in}			G	V_2

Orthogonal Line Configurations

2)		I_{in}	V_1	V_2	I_{in}	
4)	I_{in}		V_1	V_2		I_{in}
6)	I_{in}	V_1			V_2	I_{in}
-2)		V_1	I_{in}	I_{in}	V_2	
-4)	V_1		I_{in}	I_{in}		V_2
-6)	V_1	I_{in}			I_{in}	V_2

Figure 3.4: Twelve different line configurations used to take conductivity measurements. The combination of each unique configuration allows for an abundance of data to be analyzed.

The addition of two lines is not just for increasing data collection, but for redundancy purposes as well. Sometimes a measurement line breaks and is no longer useful for measuring voltage or passing current. When this happens to a μ4LP, the entire probe must be replaced because three lines are not sufficient to perform the measurement using four-line theory. Because the μNLP has six lines and performs six different measurements on contact, we can still make use of the probe even if one of the six lines is broken.

Dual Connection Pads

When taking measurements with the μ4LP, it is impossible to know if there is a break in one of the measurement lines until the data is analyzed. To fix this problem in the μNLP, connection pads are accessible on either side of the device to check for continuity before each measurement is taken. This aspect of the μNLP improves data manipulation and time efficiency by allowing the user to know if the probe has any broken lines before taking each measurement.

The additional connection pad per line not only allows for checking continuity, but adds an additional path for the current to travel from the voltage source to the probe. This insures that the lines will not heat up and melt due to the current flowing from both directions, instead of just one. At most, approximately 30 mA passes through the probe. Using both connection pads halves this value and gives an assurance that the lines stay at optimal temperatures.

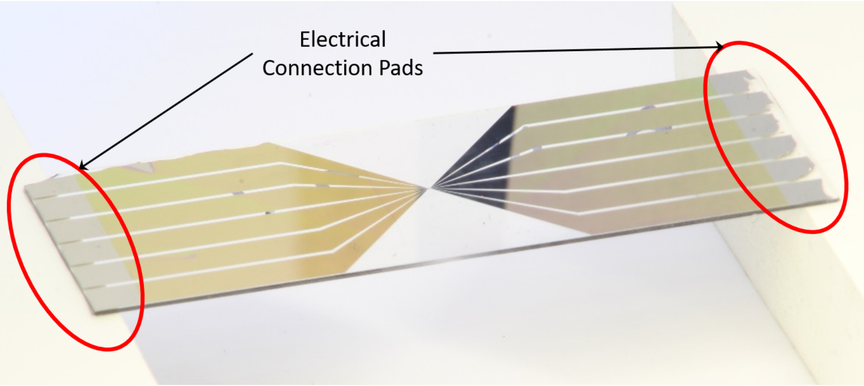

Figure 3.5: Micro-six-line probe with indicated connection pads on either side of the probe.

3.2.2 Fabrication of Micro-N-Line Probe

This section outlines the fabrication steps used to make the μNLP. To fabricate the μNLP, standard photolithography procedures are performed in a cleanroom environment provided by the electrical and computer engineering department at Brigham Young University (BYU). Figure 3.6 steps through these procedures. Many of the steps performed in this process can be found by referencing the BYU Cleanroom website [19]. A full step-by-step cleanroom process is found in Appendix A.

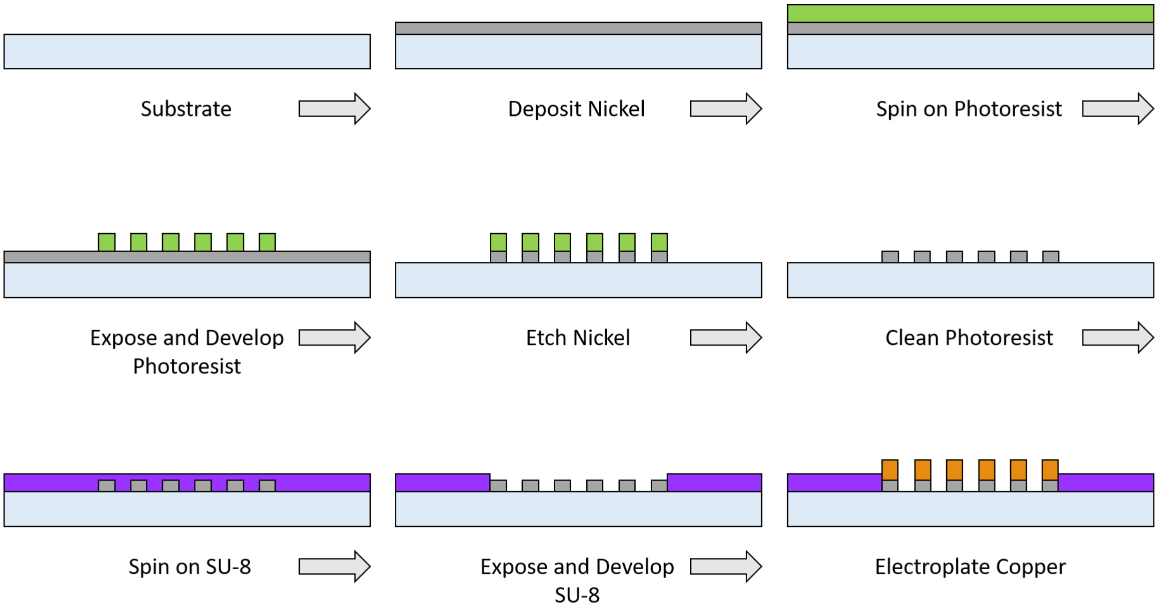

Figure 3.6: Diagram of the full fabrication process for the μNLP and μFLP.

Substrate Preparation

The BYU cleanroom is designed to accommodate a 100 mm diameter wafer. Substrates of fused silica (SiO_2) obtained from University Wafer (part #518) are used for their smooth, flat, and electrically insulating characteristics. Each wafer is 500 μm thick and is visibly translucent due to the optical properties of SiO_2. It is a desirable characteristic to be able to see through the substrate, because many of the procedures performed in this fabrication process can be checked for errors and completion by sight. See Chapter 4 for an explanation on how having a substrate that is translucent allows for measurement localization as well.

An important step between any cleanroom process is a thorough cleaning of the wafer. The wafers that come to us are generally very clean, but it has been found that they sometimes arrive with a thin layer of residue from processes they underwent before we obtained them. This can be a problem when working with thin-film layers of materials like we do. To be sure that the wafers are clean for our processes, we prepare every SiO_2 wafer in a very specific way. This is done by dipping the the SiO_2 wafer in diluted hydrofluoric acid (HF) for 30 seconds. HF is a very selective etch, in that it etches SiO_2 very readily, but not other materials such as single crystal Si. By using diluted HF, only the very outside layer of glass is etched away in the 30 seconds it is submerged, keeping the dimensions of the wafer basically the same while stripping off any imperfections and scum that might have accrued on the surface.

After the HF dip, the wafer is rinsed with DI water, dried with a nitrogen gun, and placed in an oven at 150 °C for 20 min to evaporate any trace of water that might still be left on the wafer. This cleaning process is important because the first step in the fabrication of the μNLP is to deposit a thin layer of nickel on the surface of the wafer. If the wafer is not completely clean and free of any moisture or scum, the Ni may not adhere to the surface and can peel away in the various subsequent procedures.

Nickel Deposition

A 200 nm thick layer of Ni is deposited onto the substrate using Electron-Beam Evaporation. Ni is used for its corrosion resistant properties and the readily available Nickel Etch solutions provided to us by the BYU cleanroom staff. Through experimental error, it was found that a 200 nm thick layer of Ni is an optimal thickness for our probe. 200 nm is the chosen thickness for multiple reasons. The probe will need to drop 2.5 Volts through the lines for measurement purposes. The metal needs to be thick enough to withstand the heat caused by the voltage drop and also needs to be thick enough to survive the various contacts made on the connection pads during the electroplating and testing phases. If the Ni layer is too thick (greater than 300 nm), then the Ni is likely to peel off of the SiO_2 substrate due to intrinsic stress created between the glass and Ni layers during deposition. This would ruin the wafer for all future steps of the fabrication process.

AZ3330 Photoresist Nickel Mask

The next step after depositing nickel onto the wafer is to spin on and develop a sacrificial layer of photoresist (PR) that acts as a mask for the Ni when it is etched. Spinning is the most effective way to lay down a thin, uniform layer of PR onto a wafer, as opposed to spraying or submersion, where the results can be patchy or vary in thickness. A 3 μm layer of AZ3330 PR is spun onto the wafer using a spin speed of 3000 RPM for 60 seconds. To avoid PR beading on the edges of the wafer, the wafer is spun at 6000 RPM for 2 seconds after the initial 60 second spin.

A soft bake is applied to the AZ3330 by placing the wafer on a hot plate set at 90 °C for 60 seconds. This drives out most of the solvent in the PR, solidifying it in preparation to be exposed in the photolithography step.

After soft-baking the AZ3330 PR, the wafer is placed into a Karl Suss MA150 aligner to expose it to UV light. A mask, the red portion of the LASI diagram found in Figure 3.7, is loaded into the aligner as well. This mask is a 1:1 ratio mask that is placed directly over the wafer. The mask and the wafer are then exposed to the UV light for 14 seconds.

AZ3330 is a positive photoresist, meaning that the photoresist exposed to the UV light undergoes a chemical change that makes the AZ3330 more soluble in MIF 300 developer. After the wafer is developed in MIF for 45 seconds, the PR left on the surface of the wafer is an exact copy of the mask used. The surviving pattern of AZ3330 is now the mask used to etch the Ni layer previously deposited. This AZ3330 mask is further strengthened by performing a hard-bake on it. It is placed on a hot plate at 110 °C for 60 seconds. This prepares it to withstand the chemical attack of Nickel Etch.

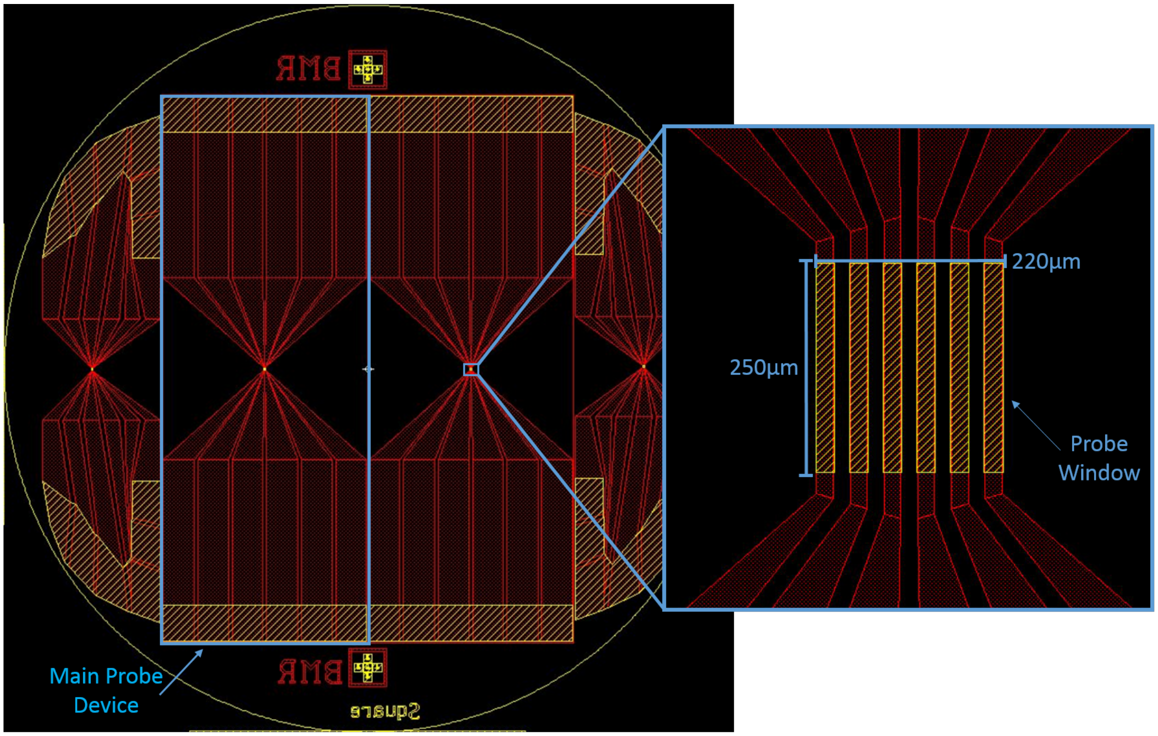

Figure 3.7: LASI7 representation of wafer mask. The red portion of the diagram represents nickel coated in SU-8, while the yellow portion represents the areas where no SU-8 is present.

Nickel Etch

The wafer, now having a sacrificial AZ3330 PR mask on the Ni layer, is then submerged in Nickel Etch kept at room temperature. Etching usually takes 5-8 min depending on temperature and if the solution is aggravated by stirring or vibration. Because the wafer is made of clear SiO_2, it is easy to tell when the etching is complete. When the parts of the wafer not covered in AZ3330 PR are completely clear, then the etch is done. This step is always validated by checking the probe through a microscope to see that there are six distinct Ni lines etched. Leaving the wafer in the Nickel etch for too long causes over-etching of the Ni lines. Special attention has to be taken in this step to be sure that the lines are etched to correct dimensions of 250 μm long × 20 μm wide, with 20 μm spacing between each line. The AZ3330 mask is then cleaned off with acetone and isopropyl alcohol to leave only the Ni that was patterned. The wafer is placed in and oven at 150 °C for 20 min after the PR is stripped off to drive off any solvent or water that might be left on the surface.

SU-8 Insulating Mask

Following the etch, a thin 0.75 μm layer of SU-8 2000.5 PR is spun onto the wafer as an insulating and protective layer that covers the whole device except for the connection pads and a window that exposes the six micro lines. One of the characteristics of SU-8 that makes it so useful in micro-structure applications is its ability to form high aspect ratio structures. For lines and trenches it has an aspect ratio of up to 15 [20]. This means that SU-8 can be used to build walls that are 15 times higher than they are wide, without any undercut.

The SU-8 is spun on in the same manner as the AZ3330, except it is spun at 1000 RPM for the 60 second interval. Like the AZ3330 PR, SU-8 PR has to undergo a soft-bake process before it is exposed to UV light. The soft-bake is performed by placing the wafer on a hot plate at 65 °C for 60 seconds, turning up the temperature to 95 °C, letting it sit for 3 min, then ramping the hot plate back down to 65 °C. This drives out most of the solvent in the SU-8 and starts a chemical reaction that hardens the SU-8 layer.

After soft-baking the SU-8, the wafer is placed into a Karl Suss MA150 aligner. A 1:1 ratio mask, the yellow portion of the LASI diagram found in Figure 3.7, is also loaded into the aligner and placed directly over the wafer. The Ni layer has alignment marks designed to make the SU-8 mask line up perfectly with the Ni pattern. Once the mask is aligned, the wafer is exposed to UV light for 30 seconds.

SU-8 is a negative PR, meaning that the photoresist exposed to the UV light undergoes a chemical change that makes it harden through cross-linking the SU-8 polymers. Exposed SU-8 is significantly less soluble in SU-8 Developer. After exposure to UV light, the SU-8 must undergo a hard-bake to complete the cross-linking process and prepare it for development. The hard-bake is performed by placing the wafer on a hot plate at 65 °C for 60 seconds, turning up the temperature to 95 °C, letting it sit for 4 min, then ramping the hot plate back down to 65 °C. This drives out any remaining solvent in the SU-8 and completes the chemical reaction that hardens the SU-8 exposed by UV light.

At room temperature its takes about 50 seconds to develop the SU-8 when the wafer is fully submerged in SU-8 Developer. The probe is then checked under a microscope to see if the window is clear of all SU-8. As well as being electrically insulating, the SU-8 layer also acts as a mold for the copper electroplating process that comes later. Each exposed line has dimensions of 250 μm $\times$ 20 μm, with 20 μm spacing, creating a window with dimensions of 250 μm $\times$ 220 μm.

Solving Current Leakage

The main reason SU-8 is used to coat the device is because it is electrically insulating. The only parts of the probe that should make electrical contact with the electrode are the metal measurement lines that make-up the probe window. Through testing, it was found that some of the devices were showing signs of current leakage from one line to another while the probe was in contact with the electrode. This meant that there were paths from one line to another through the electrode in more areas than just the dimensions of the probe window. This leakage causes false results in the conductivity measurements.

The leakage was a result of imperfections in the thin SU-8 2000.5 layer. The imperfections form pin holes in the SU-8 layer and allow for current to pass through the supposed insulating layer. These pin holes are the results of any combination of the following theories:

- The thin layer of SU-8 2000.5 is punctured by the hard surface of the electrode.
- The thin layer of SU-8 2000.5 forms holes while developing in the SU-8 Developer.
- The SU-8 mask (as seen in the yellow portion of the LASI diagram found in Figure 3.7) has imperfections on it that allows for holes to form after exposure.

To solve this problem, I came up with two solutions that are now standard procedures in the probe fabrication recipe and found in the fabrication process in Appendix A. The first solution to fixing the current leakage problem is the application of SU-8 2005 to provide a second SU-8 layer of about 5 μm. This thicker layer solves the imperfections caused by the first two theories, but does nothing to solve the last. To fix imperfections caused by the mask its self, a second SU-8 mask is used to expose the second layer of SU-8 that is spun onto the wafer. By using a separate mask to expose the second layer of SU-8, the probability of pin holes forming in the same location is very small. Through the application of a thicker layer of SU-8 with a second mask, all current leakage ceased to occur in the measurements.

Dicing The Micro-N-Line Probe

After completion of the wafer, the probe is diced into a 7.5 cm × 2.8 cm rectangle to fit the dimensions of the custom probe holder in the measurement apparatus. This is performed by using a diamond tipped dicing saw installed in a Disco DAD machine programmed to cut straight lines through the wafer. Figure 3.8 shows a diced, complete μNLP.

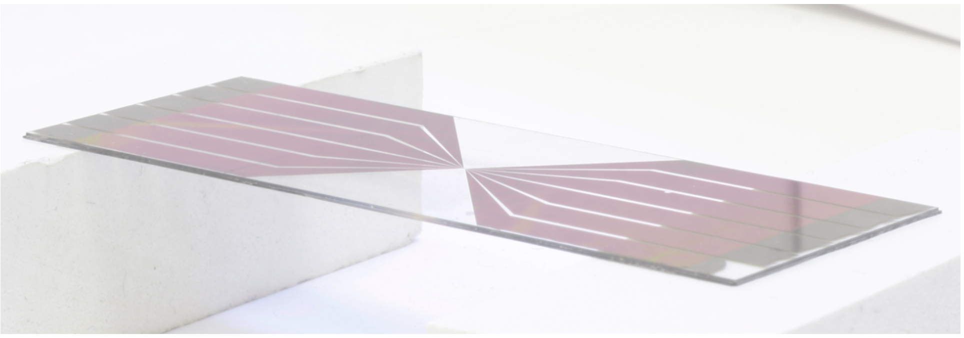

Figure 3.8: Completed μNLP. The six nickel lines are are clearly seen with the majority of the probe coated in a protective SU-8 layer.

3.3 Micro-Flex-Line Probe

3.3.1 Probe Design Improvements for Micro-Flex-Line Probe

When the testing of an electrode sample is needed in a commercial fabrication facility, a piece must first be cut from the main roll of electrode during one of the steps in the fabrication. Knowing that it is possible to correctly fabricate the μNLP, we felt it was necessary to make the probe more adaptable to taking measurements on electrodes during the electrode fabrication process without having to cut a piece off the main roll, saving time and material for the facility.

A flexible probe is a solution to making non-destructive and reliable conductivity measurements in an in-line fashion. The probe could be placed on a roller that takes measurements as the electrode moves down a belt. By fabricating the μNLP on a flexible substrate, the μFLP was developed. The flexibility assures the probe will not break due to stress, tension, or torsion, and will be able to withstand large normal forces that may occur during the testing of thin-film electrodes.

To choose the flexible substrate, probe fabrication details need to be taken into account. During fabrication, the substrate has to be able to withstand temperatures of up to 150 °C, be resistant to various chemicals such as solvents, photoresists and their developers, and Ni etch. The substrate also has to have a surface roughness on the nanometer-scale ($>$1nm and $<1\mu$m) to accommodate the micro-features created on the wafer's surface. Kapton polyimide film fulfills all of the requirements needed to create the μFLP, while also being highly durable and flexible.

A flexible substrate provides for a more durable probe as it can bend and take impacts without breaking like a glass substrate would. 150 μm thick Kapton was chosen as opposed to a thinner option for two reasons. First, the flexibility is not hindered in any way and it keeps a more rigid form when being handled, thus preventing creases in the nickel and SU-8 if over-bent. Second, thicker Kapton doesn't curl as much due to intrinsic stress created when the Ni layer is deposited onto the surface, thus preventing some complications in fabrication due to a curved wafer (these complications are discussed later in this chapter).

3.3.2 Kapton Polyimide

The purpose of this section is to introduce the reader to Kapton polyimide film to further explain why it is used as the substrate for the μFLP. Kapton is a product produced by the company DuPont and has an abundance of data collected on it [21].

Introduction to Polyimides

Polyimide films, PI films, have been used since 1955 in many different applications such as thermal and electrical insulation, flexible circuitry, purification of water, and some photolithography process, to name a few. This is largely due to its mechanical and thermal properties. PI is light-weight, strong, heat resistant, and has great flexural retention (meaning the film can bend without sustaining permanent bending) [22]. PIs are also noted for their resistance to organic solvents and dilute acids [23]. These properties arise from the molecular structure of the many polymer strands that cross-link together to form the polyimide.

To understand where the properties of polyimide film come from, we first need to understand the molecular structure of PI. Polyimides are a class of polymer that are often based on stiff aromatic backbones [24]. Imides and how they link together to form polymers will be discussed to understand polyimides.

An imide is a functional group consisting of two acyl groups bound to nitrogen. The structure as seen in Figure 3.9 is an example of an imide. It has two double bonded oxygen atoms attached to respective carbon atoms (acyl group), each in turn are attached to the same nitrogen atom which also has an attached hydrogen atom [25]. Polyimides are called as such because of the many imides that are found in the polymer strands.

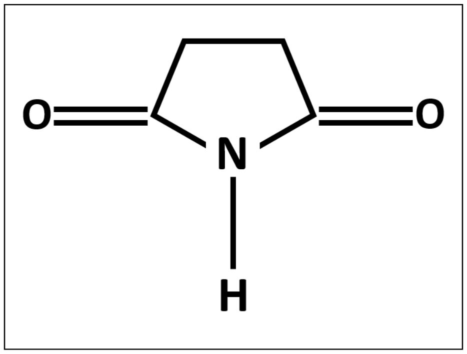

Figure 3.9: Basic structure of an Imide molecule.

Synthesis of Polyimide Film

Figure 3.10 shows the step by step process of reactions that lead to polymerization of Kapton PI [26]. It is worth noting that there are many different kinds of PI, and the figure shows the polymerization of Kapton PI only.

Dianhydride and a diamine are molecules that react at ambient conditions (equilibrium reaction) in a solvent to form poly(amic acid). This reaction is almost irreversible due to the high molecular weight of the poly(amic acid) [27]. It is then dehydrated, usually through heat, to cyclisize (one part of the molecule becomes linked to another to form a closed ring) into the final Kapton PI form. An imide is found on the far left of the final Kapton structure. With more heat applied to the system, the PI strands cross-link together to form long polymers as the solvent is driven out. These long polymers connect to each other by forming bonds between the aromatic

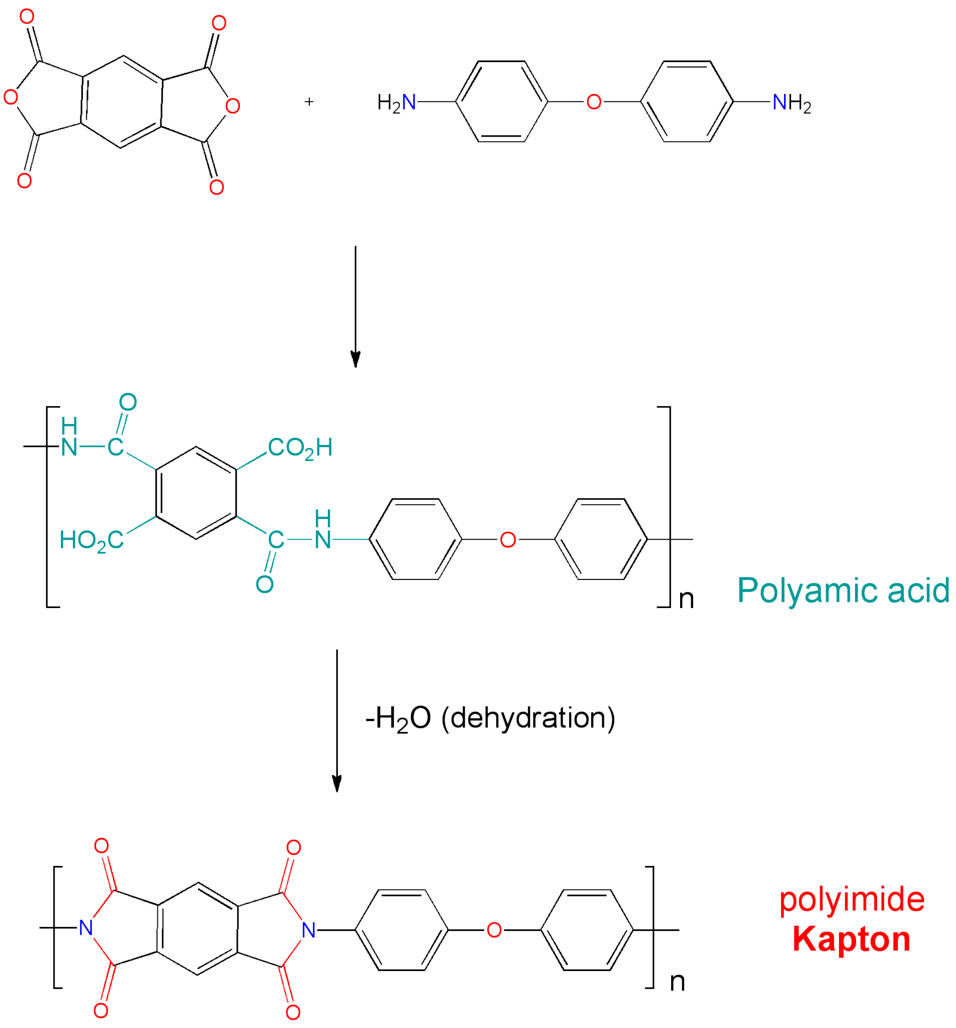

Figure 3.10: Step by step reaction scheme of how Kapton polyimide is synthesized. Top left is a dianhydride molecule, top right is a diamine molecule, middle is the poly(amic acid) that then dehydrates into Kapton PI. The subscript n outside the brackets in the figure indicates that the structure repeats its self an indeterminate amount of times.

rings and the double bonded oxygen and branch off to form a large network of polymers that become the Kapton film used.

Thermal Properties of Kapton

Table 3.1 shows the thermal properties of Kapton film as seen in the DuPont General Properties form for Kapton [22]. As we can see, Kapton has a small thermal expansion coefficient (α), low thermal conductivity (C_v), and very low shrinkage.

Table 3.1: Thermal Properties of Kapton, 25μm thick [21].

Thermal Property	**Typical Value**	**Test Condition**
Thermal Expansion Coeff.	$20\ \frac{\text{ppm}}{^\circ\text{C}}$	-14–38°C
Thermal Conductivity	$2.87\times10^{-4}\ \frac{\text{cal}}{\text{cm}\cdot\text{seconds}\cdot^\circ\text{C}}$	23°C
Shrinkage	1.25 %	120 minutes @ 400°C
Glass Transition Temp.	360–410 °C	N/A

The thermal properties of Kapton are impressive. Kapton can withstand extremely high temperatures of up to 300°C while transferring very little of the heat. This means it can be used as a very efficient substrate for our probe, as it will have to withstand high temperatures during the fabrication process. Because of its small shrinkage percent, we know that Kapton will hold shape under a range of temperatures from -270°C to 400°C [23]. These properties makes it ideal for the μFLP, because bending and shrinking will affect photolithography steps in the fabrication process.

Physical Properties of Kapton

It is well known that Kapton is a polyimide film with phenomenal physical properties. Table 3.2 shows some of the physical properties of Kapton film as given by DuPont [22].

Table 3.2: Physical Properties of Kapton, 25μm thick [21].

Physical Property	**Typical Value**
Ultimate Tensile Strength	231 MPa
Impact Strength	78 N·cm
Tear Strength	7.2 N
Folding Endurance	285,000 cycles

Flexibility is one of Kapton's most familiar physical properties. Not only is it able to be folded hundreds of thousands of times before snapping, but it can withstand immense stress as well which contributes to its flexibility and strength. From a Stress-Strain Curve for 25μm thick Kapton film that is found in the DuPont data sheet for Kapton, see that Kapton can endure around

70% elongation before reaching its elastic limit [22]. Past this point the film enters the plastics regime and could tear.

The physical properties of Kapton show that it is both tough and flexible. This is far more so than normal everyday plastic such as polyethylene. The aromatic rings in Kapton adds a lot of structural support that isn't found in polyethylene. Plastic is formed only by monomers of two bonded carbon atoms each with two respective Hydrogen atoms. This structure can't withstand the kinds of stress, impact, and folding tests that Kapton can endure quite easily. These are some of the mechanical reasons why we are using Kapton and not polyethylene for the substrate of the μFLP.

Conclusions on Kapton Film

Kapton film is the best option when it comes to heat resistance and physical durability. The unique aromatic rings in Kapton, coupled with imides provide structure and bonding points for the Kapton polymers to form a strong, flexible, heat resistant sheet.

3.3.3 Fabrication of Micro-Flex-Line Probe

Theoretically, the only difference between the μFLP and the μNLP is the substrate that the probe is built upon. The μFLP has a flexible Kapton film as the substrate, instead of the previously mentioned fused silica used for the μNLP. It is fabricated using the same steps explained for the μNLP, except for a few minor alterations to the process caused by the exchange in the substrate. This section explains the minor, but important modifications made to the fabrication process in order to make the μFLP as shown in Figure 3.11.

Pre-Bake of Kapton Film

Kapton film is extremely resistant to heat, making it an ideal material when having to use temperatures up to 150 °C. Though the film is very heat resistant, it was found through experimental error that the Kapton wafer shrinks slightly throughout the fabrication process. To prevent this shrinkage affecting the final stages of the probe fabrication process, the Kapton is pre-baked

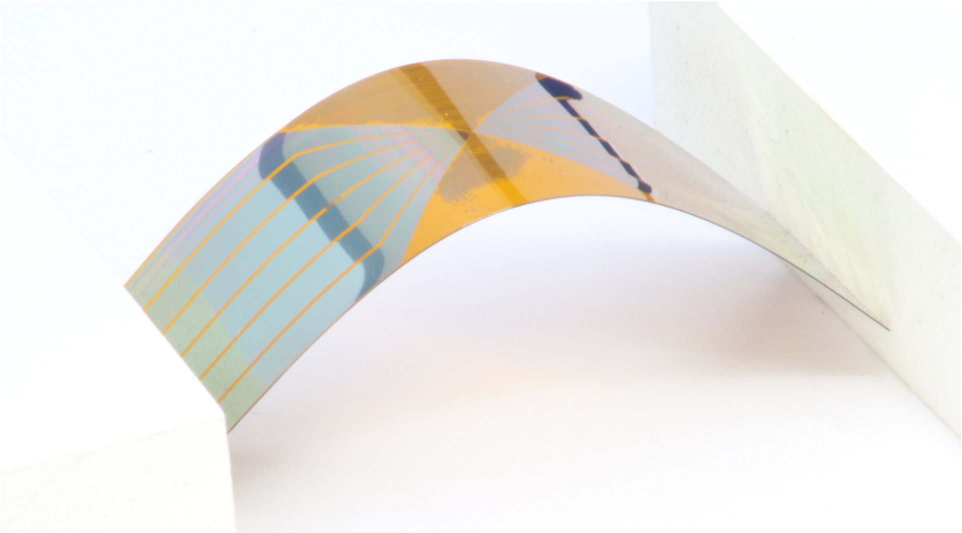

Figure 3.11: Completed μFLP displayed to show that the probe is flexible. The orange tint is due to the coloring of the Kapton substrate.

to shrink the film before the first step of depositing nickel. The pre-bake is performed by placing the polyimide on a hot plate or in an oven set at 150 °C for 15 min.

Mounting Kapton To a Rigid Wafer

Throughout the fabrication process, the substrate of the wafer makes contact with various vacuums, hot plates, and holders in several different steps. It is possible to go through the whole fabrication process for the μFLP using just the Kapton polyimide substrate as the surface that makes contact, but it adds two complications in performing some of the process steps.

The first complication comes from the frequent use of vacuums in many of the fabrication steps. Spinning on PR, cleaning the wafer, and all the photolithography steps require the use of vacuums to hold the wafer in place. Because the Kapton wafer is flexible, it conforms to the grooves of the vacuum causing the wafer to no longer have a completely flat surface. It is important to have a uniformly flat surface during the steps where material is being spun on. If the surface isn't flat, then the spun on layer isn't uniform across the wafer and creates complications down the line in etching and developing steps. It is also important to have a uniformly flat surface during the photolithography steps. If the wafer is conforming to the grooves of the vacuum the UV light will not hit the wafer at a normal angle, causing the PR not to match the mask being used after development.

The second complication is due to the previously mentioned bending of the flexible wafer caused by intrinsic stress between the Ni layer and polyimide. The intrinsic stress results in the wafer curving into a taco-like shape. Many of the steps following nickel deposition require the wafer to be placed on a hot plate for curing PR, but the curved nature of the wafer results in a non-uniform bake on hotplates. To try and fix this problem, a metal ring was created to fit the outer parameter of the Kapton wafer to make it lay flat on the hot plate during baking steps. This worked in helping the wafer to receive uniform heat from the hot plate, but an undesired outcome was that the ring would essentially be glued to the outer perimeter of the wafer. Many wafers were destroyed in trying to separate the ring from the Kapton wafer.

To remedy both these complications, the Kapton polyimide film is mounted onto a rigid wafer to make fabricating the μFLP as similar and easy as processing the μNLP. By mounting the Kapton to a rigid wafer, it eliminates all curving of the film, allowing for uniform heat transfer on a hot plate, and removes all uniformity complications caused by the vacuums.

Various methods failed in attempting to mount the Kapton wafer to a rigid wafer for ease-of-use in the fabrication steps. One method was to try and use super glue to fuse the two wafers together. This method worked very well to mount the Kapton and left almost no air bubbles, but was extremely messy and nearly impossible to take off the rigid mount. Another method was to use AZ2020 PR as a glue, but it left large air bubble and came off during random steps in the fabrication. Finally, the mounting process was successfully achieved by using Parafilm as an adhesion layer between the polyimide wafer and the rigid mount.

Traditionally, Parafilm is used as a temporary seal for chemical containers such as beakers and petri dishes, but has been found to be an effective adhesive of two flat substrates to each other. In addition to Parafilm being a great adhesive, it is extremely chemical resistant and very easy to handle. It can withstand any of the developers, etch solutions and temperatures used in the full fabrication process. This procedure was discovered by myself and has been extremely useful in the adhesion of Kapton to a rigid wafer. When the Parafilm is heated to 90 °C, it creates an airtight seal between the two wafers. A few air bubbles may be present at first, but they usually dissipate and don't effect the spinning or photolithography steps. To remove the Kapton from the rigid wafer at the end of the fabrication process, only a few drops of acetone between the Kapton and Parafilm is enough to peel off the polyimide with ease.

Cutting the Micro-Flex-Line Probe

After the fabrication of a probe, it needs to be cut to the desired dimensions needed to fit its custom holder. For the μNLP, this is done with a diamond blade that needs to be mounted into a machine that is programmed to cut the wafer in a very specific way. This is time consuming, and sometimes the blade rips up the SU-8 and Ni on the wafer. This can ruin the device, rendering it useless in the testing the conductivity of thin film electrodes. All this is bypassed when using the flexible Kapton as the substrate of the probe.

After the μFLP is fabricated, it is easy to cut it to the necessary dimensions to fit it into the custom holder. Kapton polyimide film can be cut with a normal pair of scissors. This essentially removes a fabrication step from the total process and safeguards the wafer from a step that could potentially ruin the wafer.

3.4 Electrodeposition of Probe Lines

The last process in fabricating a probe is to bring the six lines inside the window to a level slightly above the SU-8 to ensure contact with the electrode during measurements. To do this we use an electrodeposition process, utilizing the circuit in Figure 3.12. Copper is electroplated onto the nickel lines using a solution of cupric sulfate and sulfuric acid. 3-mercaptopropanesulfonic acid (MPSA), polyethylene glycol (PEG), and sodium chloride are added to the copper solution to facilitate smooth, “Bottom-Up” filling as described by Tan et al. [28].

3.4.1 Performing Electrodeposition

A few drops of the copper solution is place on the window to provide the copper ions needed to plate up the Ni lines. Plating is achieved by applying a voltage difference (V_E) between a probe line and the copper lead, which are connected by the plating solution. This voltage difference drives the copper ions to form copper metal on the the Ni. A micro-controller is used to ensure accurate deposition. The code running the micro-controller calculates the necessary mass needed

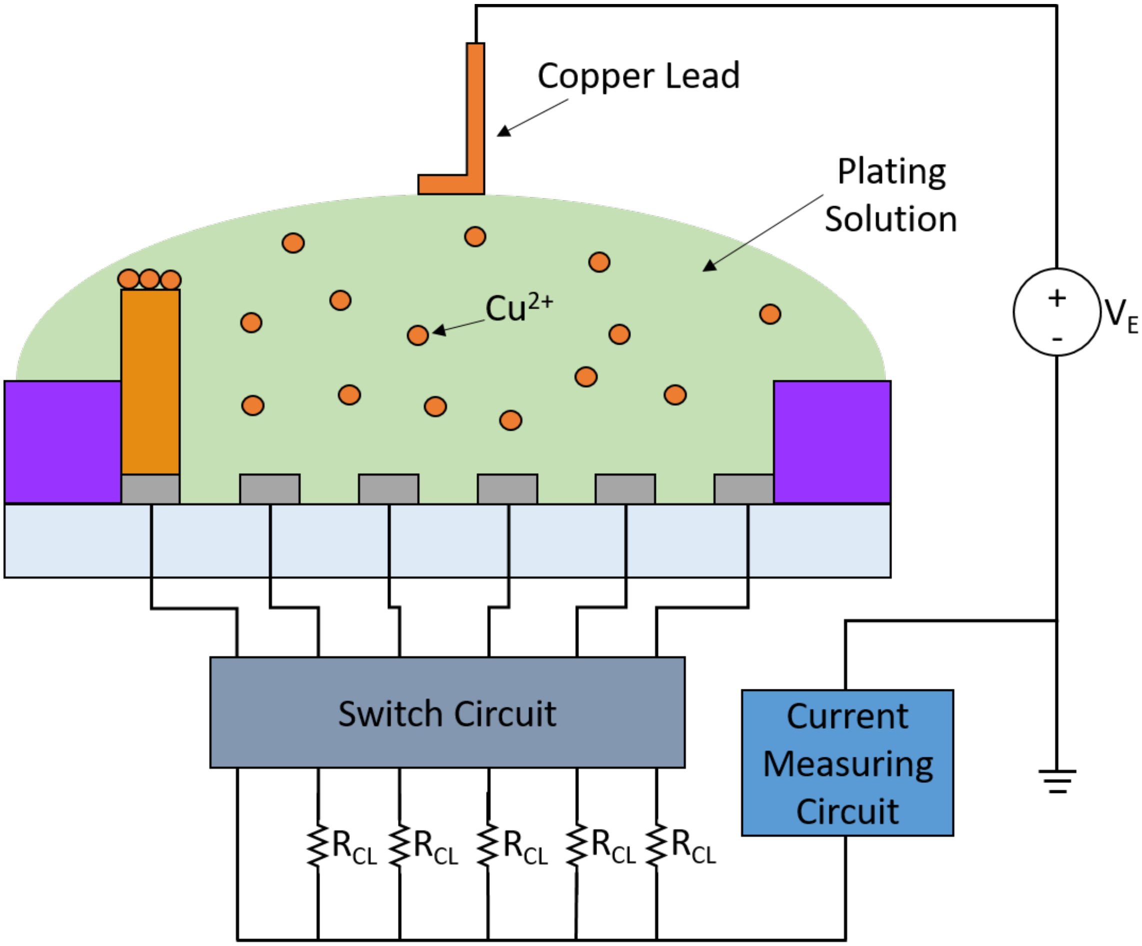

Figure 3.12: Schematic of how electroplating is performed on each of the lines in the probe window. A voltage difference (V_E) is applied between a line and the copper lead, which are connected by the plating solution. The voltage difference provides the means for the copper ions (Cu^{2+}) to form copper metal on the nickel line. The other five lines are each in series with 150K Ohm, current limiting resistors (R_{CL}) to limit current flow to near zero, and keep them from having floating voltages.

to plate to the desired height, then converts that number into coulombs. Once the number of coulombs is reached through plating, the controller set V_E to zero. Coulombs can be counted and calculated by following Equation 3.2, where C is the number of coulombs. One coulomb is the charge transported by a constant current of one ampere for one second.

$$1\ \mathrm{C} = 1\ \mathrm{A} \times 1\ \mathrm{second} \tag{3.2}$$

By analyzing profiles like the one see in Figure 3.13, it can be noted visually how much each line needs to be individually plated over a few iterations to bring them to the desired height. After all the lines have reached a height of approximately 1–2 μm above the SU-8 mold, the probe is ready for testing conductivity of thin-film electrodes.

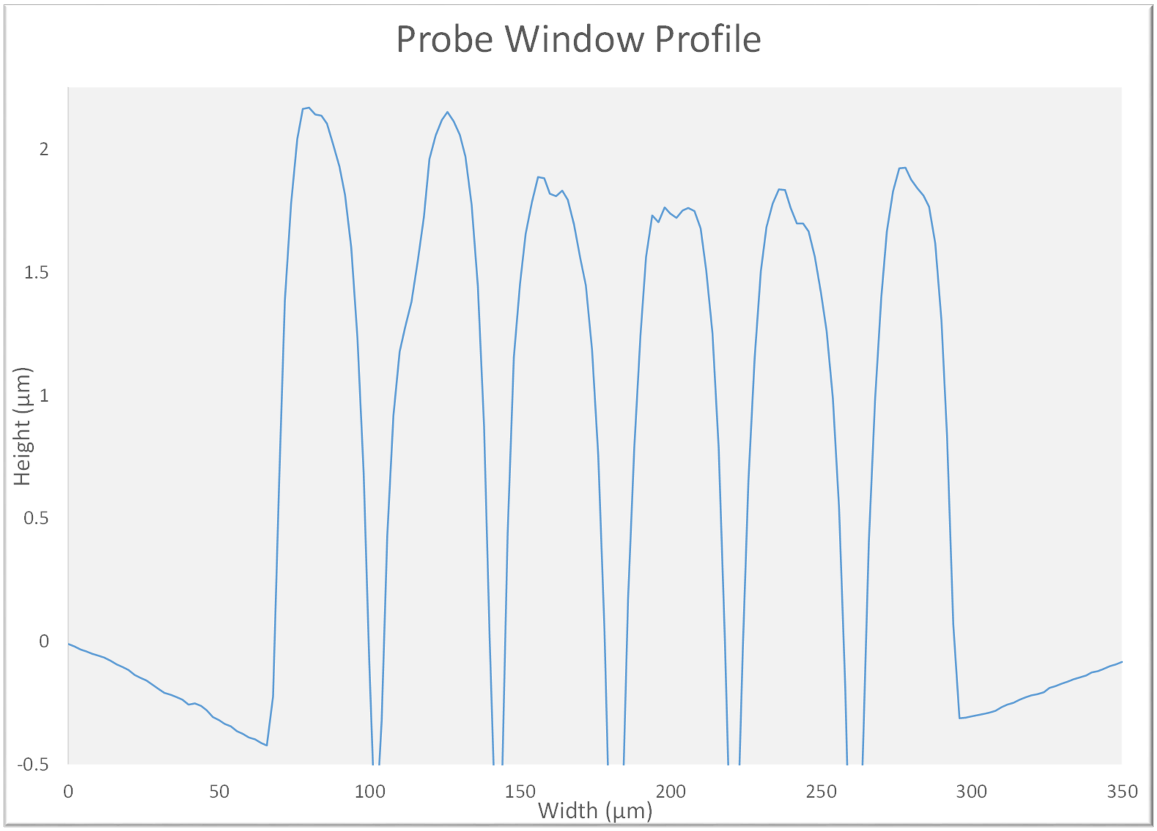

Figure 3.13: Profile of a μFLP taken with a profilometer.

3.4.2 Designing the Electroplating Stage

The stage used in the electrodeposition process has two functions: to hold the probe in place, and to complete an electrical connection from the positive lead to ground.

Figure 3.14 shows a previous method used to hold the probe in place and complete the circuit. Double-sided tape is used to hold the probe on the mount and alligator clips are used on the connection pads to complete the circuit. While this method does work, it is hard to remove the probe from the tape, sometimes snapping the μNLP from the stress of removal. The alligator clips sometimes crack the glass at the location of the connection pads on the μNLP or puncture the substrate on the μFLP. This has lead to many probes breaking during this last stage of fabrication.

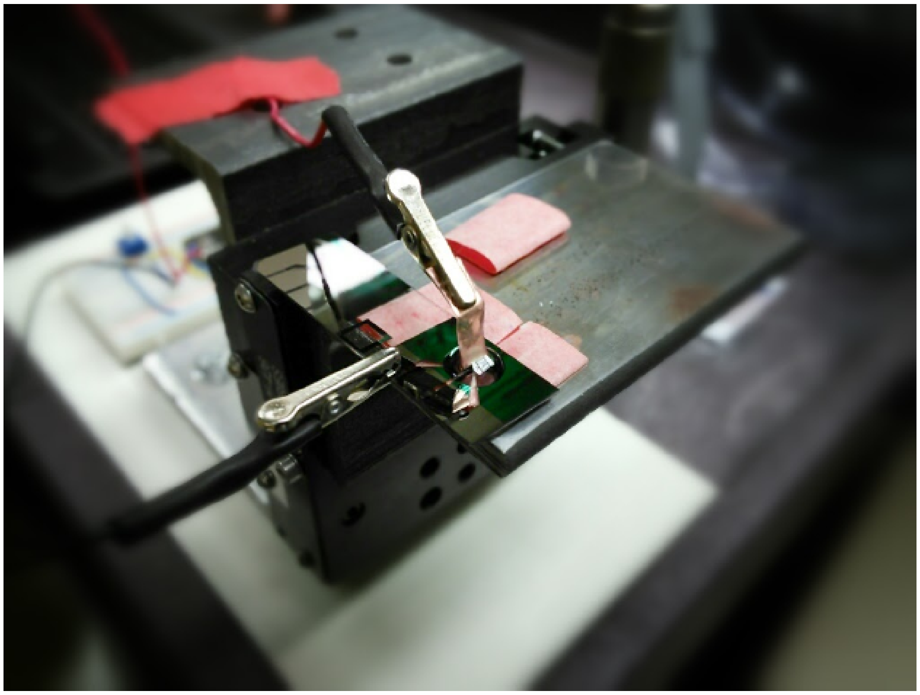

Figure 3.14: Old stage used to hold the probe undergoing electrodeposition. Alligator clips are used to close the electrical circuit and tape is used to hold the probe in place. The probe seen in this figure is a practice probe meant to experiment with electroplating.

To increase the throughput of finished probes, a new electroplating stage was developed by myself to ensure that no more probes break during this step. Figure 3.15 shows the new stage that was designed to make electroplating easier and less destructive. There are 6 copper spring leads that act as both the method to hold the probe in place and complete the circuit. All six lines are controlled by a switch relay circuit, as depicted in Figure 3.12. One line is connected to ground, while the other five lines are in series with high-ohm current-limiting resistors (R_{CL}) to restrict the passage of current and remove floating potentials. The ability to switch between the lines without having to physically change a connection to the probe ensures a low probability of breaking the probe during this step.

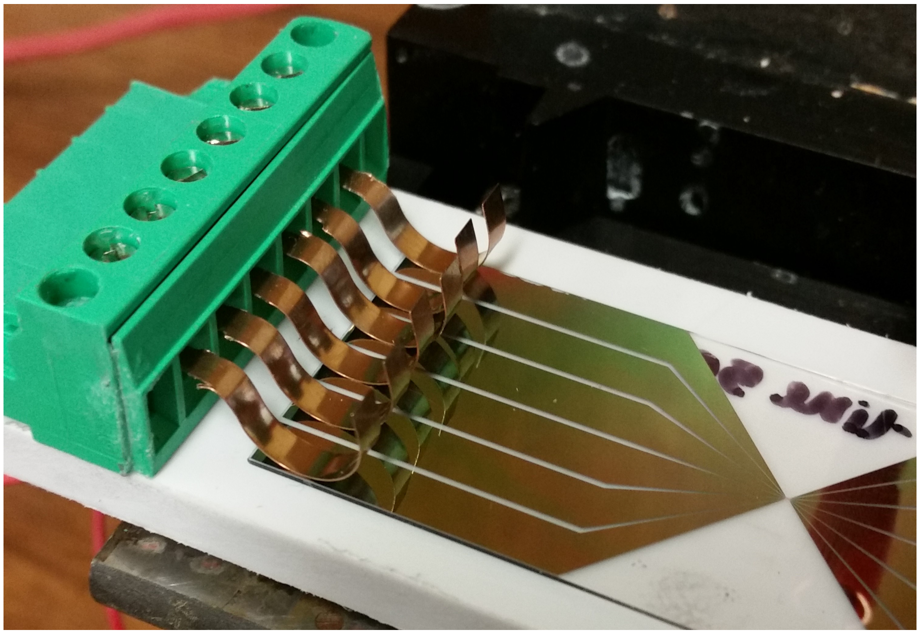

Figure 3.15: New stage used to hold the probe undergoing electrodeposition. A custom mount with copper springs are used to hold the probe in place and close the electrical circuit.

3.5 Conclusion

The designs of both the μNLP and μFLP were successfully realized by analyzing and making necessary changes to the μ4LP. Fabrication of these two probes were completed at the BYU cleanroom facility and tested to be robust, functioning devices. The rigid μNLP pathed the way to developing the flexible μFLP. Both probes provide six measurement lines, which adds an increased number of measurements made per contact with the electrode surface, as well as giving the user more options if a measurement line were to break or loose contact. The flexible μFLP will provide battery electrode manufacturers with a durable conductivity probe that can adapt to any planar surface, roller or wheel that might be used in the process. This allows for non-destructive, in-house conductivity measurements.

CHAPTER 4. ADAPTATION OF MEASUREMENT APPARATUS

4.1 Introduction

This chapter outlines the modifications, developments, and construction of the two measurement apparatus used to house and maneuver the μNLP and μFLP. The first half of this chapter focuses on the modifications made to the measurement apparatus that houses the μNLP, while the second half outlines the development and construction of the custom built measurement apparatus that houses the μFLP. Both apparatus are noted to be functional and efficient, but the purpose of this chapter is to stress the capabilities and usefulness of the measurement apparatus used to make measurements with the μFLP possible.

4.2 Measurement Apparatus

The measurement apparatus used to gather data with the probes consists of four components:

1. Three-Axis Stage
2. Custom Probe Holder
3. Data Acquisition Circuit
4. Force Sensor Circuit

A MATLAB script written by John Vogel is used as the master code that controls the entire measurement apparatus from the movement of the stage to the acquisition and storage of the data collected. Figure 4.1 is a representation of the measurement apparatus. This section will outline the basics of each of the four components of the measurement apparatus and how they contribute to taking measurements with the probe.

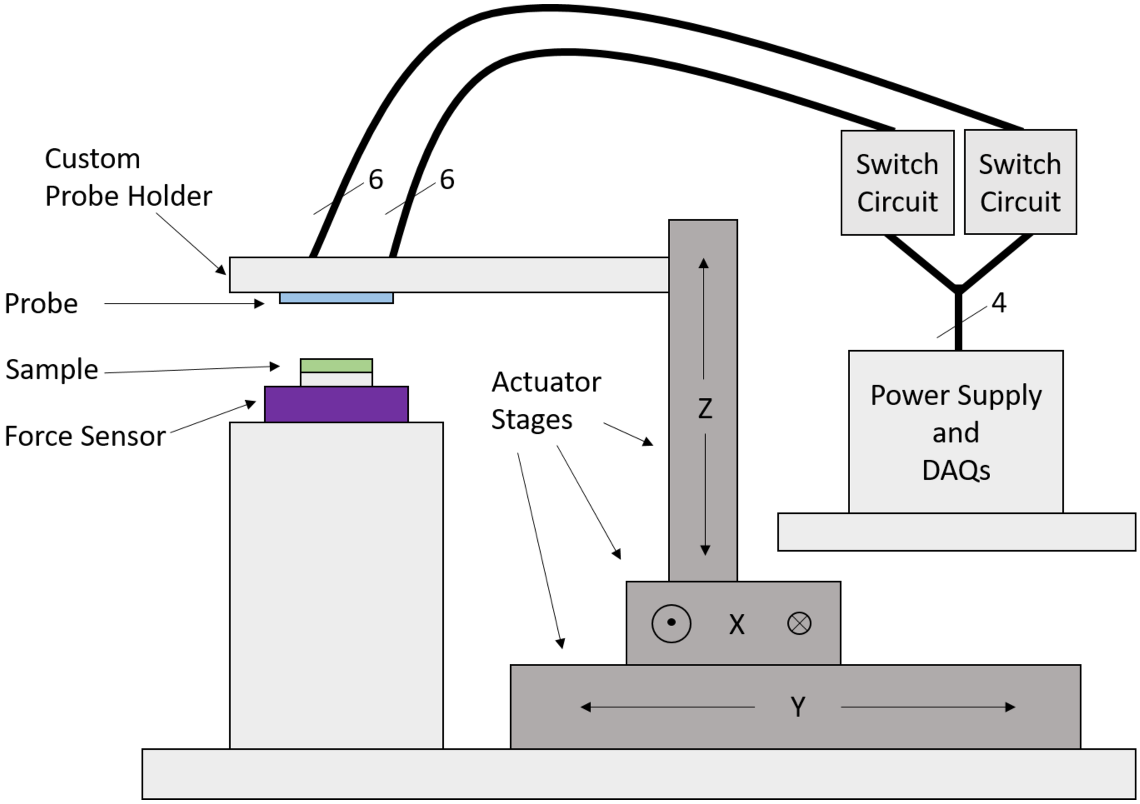

Figure 4.1: Schematic of the three-axis measurement apparatus used to conduct high resolution conductivity maps of thin-film battery electrodes.

4.2.1 High Resolution Three-Axis Stage

The stage used to circumnavigate the electrode in order to create high-resolution conductivity maps is a Newmark Systems XYZ stage. The stage has nanometer-scale accuracy in all three of the X, Y, and Z directions. Usually, this hardware is controlled by LabVIEW software, but the master MATLAB code generates commands that mimic LabVIEW commands.

4.2.2 Custom Probe Holder

Attached to the stage is a custom probe holder attached to a mount on the Z-axis motor shaft. This allows for up/down movement of the probe, while the X-axis and Y-axis motors allow the probe to be moved in the other two dimensions to make a map of the electrode. The probe holder is made out of 3D printed plastic to custom-fit the probe and stage mount. 3D printing gives us the ability to modify the holder and print it at will to meet the required alterations that may be made to the stage or probe.

4.2.3 Data Acquisition Circuit

Our data acquisition circuit uses four Agilent 34450A Digital Multimeters that all feed their data into a computer via USB connections. One measures the voltage going into the electrode from a PS280 DC power supply (V_{in}), another measures the current passing through the electrode (I_{in}), and two measure Voltage 1 (V_1) and Voltage 2 (V_2). These four measurements can be referenced in Figure 3.3. Each of the digital multimeters are commanded by the master code when to record a measurement. The data obtained is dynamically stored in an Excel spreadsheet as the measurement is taking place. Inversion software previously developed is used to interpret the data and plot a map of conductivity [17].

4.2.4 Force Sensor Circuit

Installed on a stationary pedestal directly below the probe holder is a Transducer Techniques MLP-100 force sensor. This force sensor measures the force applied to the electrode by the probe during a conductivity measurement. A National Instruments (NI) 9237 4-channel Module inserted into a NI 9171 CompactDAQ USB Chassis together translate the signals coming from the MLP-100 into readable force measurements.

The master MATLAB code commands the Z-axis of the stage to slowly and continuously move the probe down onto the electrode until a force of 15 lbs is reached. When this force is reached, the stage uses a proportional integral derivative (PID) controller loop to hold the probe at that force, until the measurement data is collected. Having the master code link the force sensor and Z-axis together ensures that the probe applies the same amount of force onto the electrode sample on each measurement, eliminating any variability that might arise from data collected from differing applied forces.

4.3 Modifications to the Measurement Apparatus to Accommodate the Micro-N-Line Probe

The μNLP is a device with very specific dimensions as noted in Chapter 3. In order to make measurements, it is necessary to have a stage that is designed specifically for the μNLP. This section outlines the changes made to probe holder and the data acquisition circuit (as described above) in order to accommodate the μNLP. These changes make it possible to accurately use the probe to make high resolution conductivity maps of electrodes. Figure 4.2 shows the stage and custom probe holder components of the measurement apparatus.

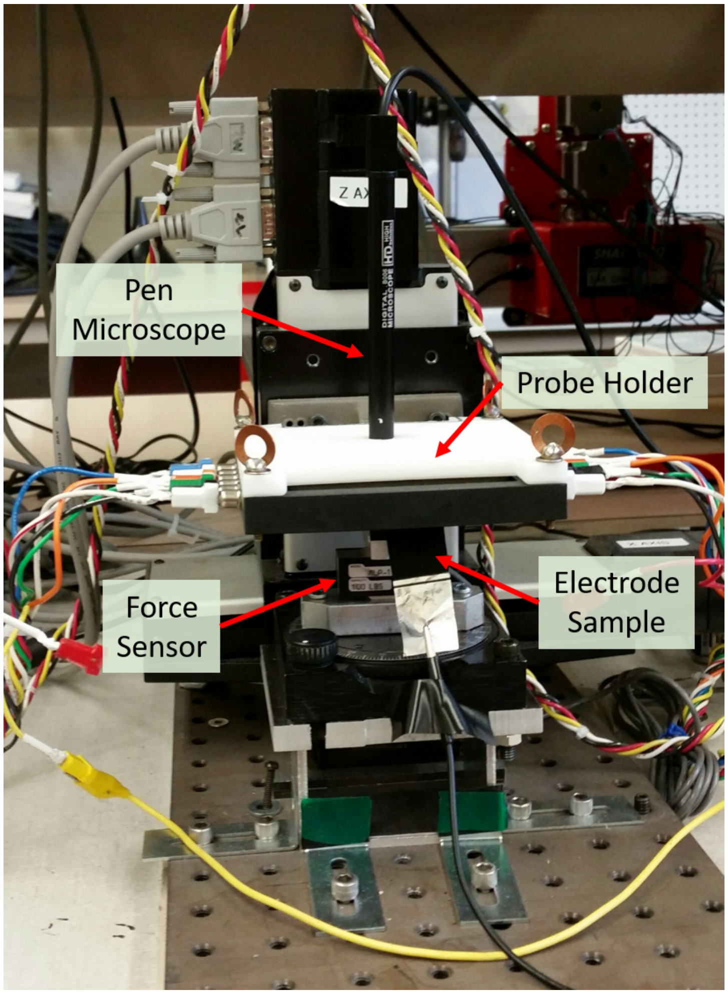

Figure 4.2: Three-Axis measurement stage used to conduct high resolution conductivity maps of thin-film battery electrodes.

4.3.1 Probe Holder Modifications to Assist the Micro-N-Line Probe

In past work, the holder used for the μ4LP was specifically made for a probe with 4 lines. Two more lines need to be taken into account when using the μNLP. In addition to the added two lines, each of the lines on the μNLP are electrically coupled to connection pads on either end of the device. To accommodate six lines and the dual-sided connection pads, the holder was completely redesigned using a CAD program, then 3D printed in-house.

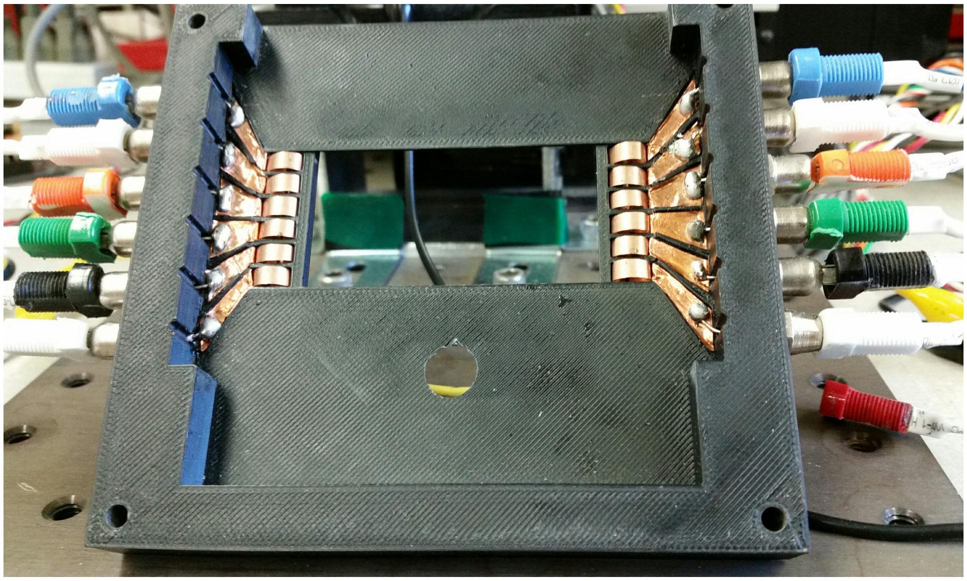

Figure 4.3: 3D printed probe holder for the μNLP. There are six copper connection pads on either side of the holder to make an electrical connection to the probe.

The probe holder for the μNLP is seen in Figure 4.3. We use six copper spring pads on either side of the holder to make an electrical connection with the probe. Each of the pads respectively have an electrical connection to one of the banana clip wires leading out of the probe holder. The six lines are then fed into the data acquisition circuit that interprets and stores the measurements. On each measurement, every measurement line of the probe is tested for continuity from one side of the holder to the other to check that none of the lines are broken.

An Accfly USB pen microscope was fit into the probe holder in order to see both the probe window and the surface of the electrode. The pen microscope can be seen protruding from the probe holder in Figure 4.2. Because the μNLP has a transparent glass substrate, it allows for the ability to localize the measurements made with the probe. By marking the surface of the electrode, measurement maps can be started in the same location even if a probe is replaced or the electrode is moved. Figure 4.4 shows an image taken with the pen microscope that shows both the probe window and the electrode surface beneath the probe substrate.

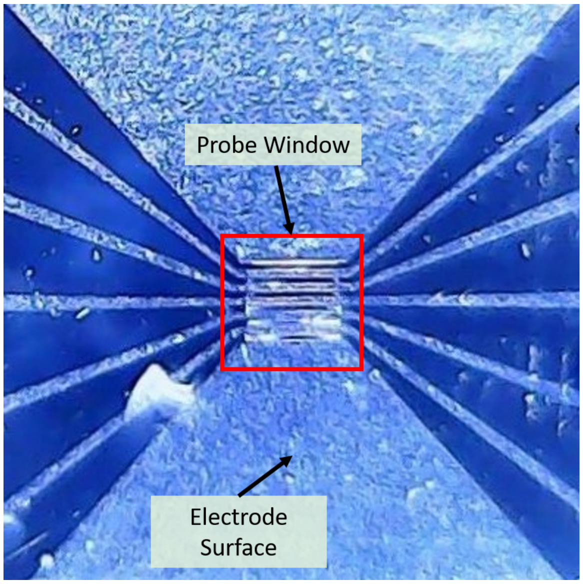

Figure 4.4: Image captured by the pen microscope attached to the probe holder. The probe window is seen just above the surface of the electrode. The electrode is visible through the glass substrate of the probe, making measurement localization possible.

4.3.2 Data Acquisition Circuit Modifications to Assist the Micro-N-Line Probe

Each of the six lines can either measure voltage, be a current source, or connect to ground in any given measurement. To successfully take a measurement, only four multimeters are needed. These four multimeters may only be respectively connected to four lines at a time, and are each programmed to only perform their specific role in measuring V_{in}, I_{in}, V_1, or V_2. This poses a complication when each line can potentially be connected to any one of the multimeters for any given measurement. To solve this problem, a switch system was designed to dynamically switch any line to any of the multimeters. Figure 4.5 shows a circuit board and schematic designed to accommodate the six modular lines of the μNLP.

The six lines coming from the probe holder feed in to a DMUX circuit that can route any of the six lines to any one of the four multimeters. Each of the DMUX's are powered and controlled

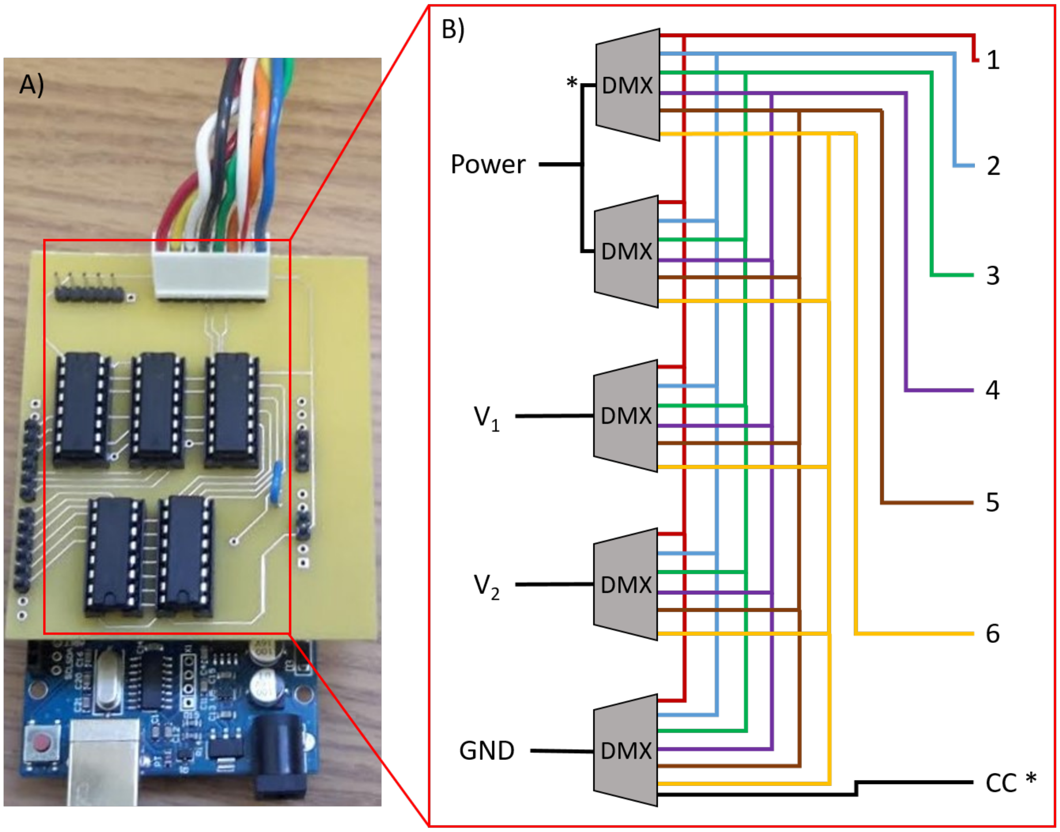

* Used Only In Orthogonal Measurement

Figure 4.5: A DMUX circuit controlled by an Arduino Board allows relay switching of connections between the measurement lines and the multimeters. This setup can support up to eight measurement lines.

by a Arduino Uno Board that receives instructions from the master MATLAB code that controls the entire measurement apparatus. There are two of these circuits in the data acquisition circuit. One is connected to each side of the probe holder to electrically connect the dual connection pads on the μNLP.

4.4 Design and Construction of Micro-Flex-Line Probe Measurement Apparatus

To make electrode research progress faster, we decided to parallelize the data collected through the conductivity measurements by using two measurement apparatuses. We decided it was necessary to build a new stage, but we didn't want to pay upwards of $30,000 for the same stage and other electrical components. Instead, we decided to build a whole new measurement apparatus as seen in Figure 4.6 and keep the price at a fraction of the cost of building an identical set up used for the μNLP. This new apparatus is dedicated to the μFLP and was built for about \$1,900 in total. For this dramatic cut in cost, very little is lost in functionality and accuracy, but much is gained in portability and ease of use. This section outlines the design and development of the new stage, probe holder, force sensor circuit, and data acquisition circuit designed for accommodating the μFLP.

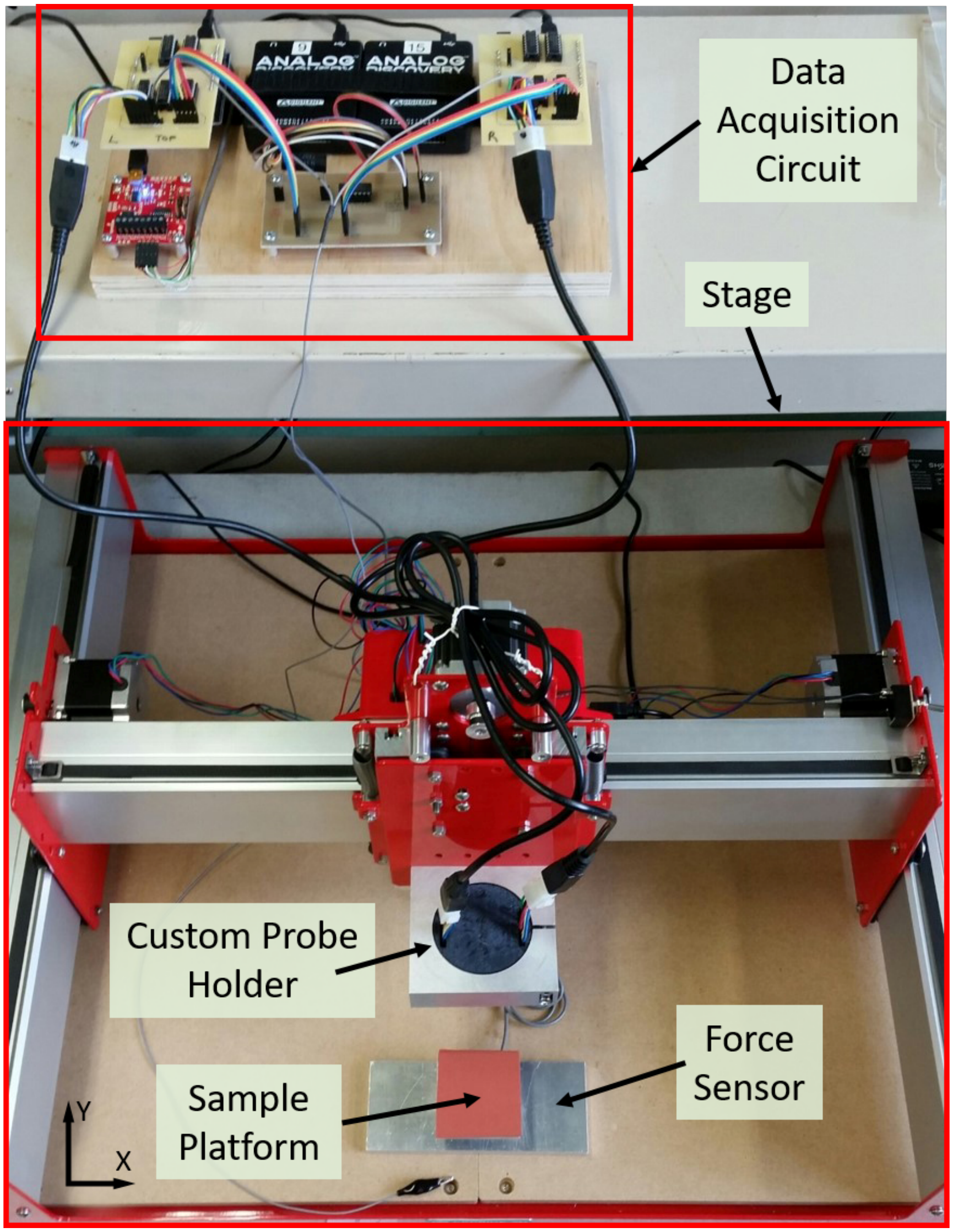

Figure 4.6: Stage developed for the μFLP.

4.4.1 Development of the Micro-Flex-Line Probe Stage

Having a stage that can be controlled and automated to move in the X, Y, and Z directions is key to producing a conductivity map of thin film electrodes in an accurate and time efficient manor. Many different XYZ stage designs were taken into account in deciding which kind of stage would be best suitable for the μFLP and provide the necessary functionality. For its price, durability, and accuracy in the X and Y directions, the Shapeoko CNC Stage was chosen to be the new stage to be used in the measurement apparatus.

The Shapeoko CNC Stage, as seen on the bottom half of Figure 4.6, was purchased from SparkFun Electronics for a little less than $1,000. It is simple to assemble and is very aesthetically pleasing. its design purpose to hold and move a CNC drill is ideal for moving our probe around efficiently in all directions with an accuracy of 0.01 mm. Although this stage cannot reach movements of only nanometers, like the Newmark Systems XYZ stage, it has enough accuracy to make high resolution maps of conductivity.

Like the Newmark stage, a master MATLAB code sends G-Code to the controller on the Shapeoko stage that controls the stepper motors on the three axis. This includes varying the speed of the Z-axis motor, when telling it to move the probe down in order to make contact with the electrode, allowing 15 lbs of force to be reached gently.

4.4.2 Development of Custom Micro-Flex-Line Probe Holder

When working with a flexible device like the μFLP, there is more leniency in designing a custom probe holder. The flexible nature of the μFLP allows for the holder to be virtually any shape or size in relation to the probe dimensions. Figure 4.7 shows the final design of the 3D printed holder. 3D printing allows for quick changes and and delivery to save time by maximizing iterations of design ideas.

As mentioned before, the Shapeoko stage is originally designed for housing and maneuvering a cylindrical milling tool. For this reason, the μFLP holder has a cylindrical protrusion with a key that the stage mount clamps onto. Pressure on all sides from the circular clamp keeps the holder in place, while the key protrusion keeps the holder from rotating. The μFLP holder can be seen attached to the stage mount on the bottom half of Figure 4.8.

Figure 4.7: Custom 3D printed probe holder designed to house the μFLP.

To utilize the flexibility of the μFLP, the holder has two curved sections (where electrical connections are made) on either side of a small flat area (where the probe window is centered for measurements). This design increases the measurement area of the electrode to be any size because the probe holder is now free standing. This is a huge improvement compared to the μNLP holder that constrains the testing area due to the inner walls of the holder seen on the top half of Figure 4.8.

The μNLP slips into the holder on either side of the flat testing area in a card slot fashion using gold-plated Molex pins. The Molex pins act as both the mechanism to hold the flexible probe in place and as electrical connections to the probe. The sliding action to insert the probe also cleans the connection pads of any oxide that might have built up over time, ensuring a clean electrical path every time the probe is inserted into the holder.

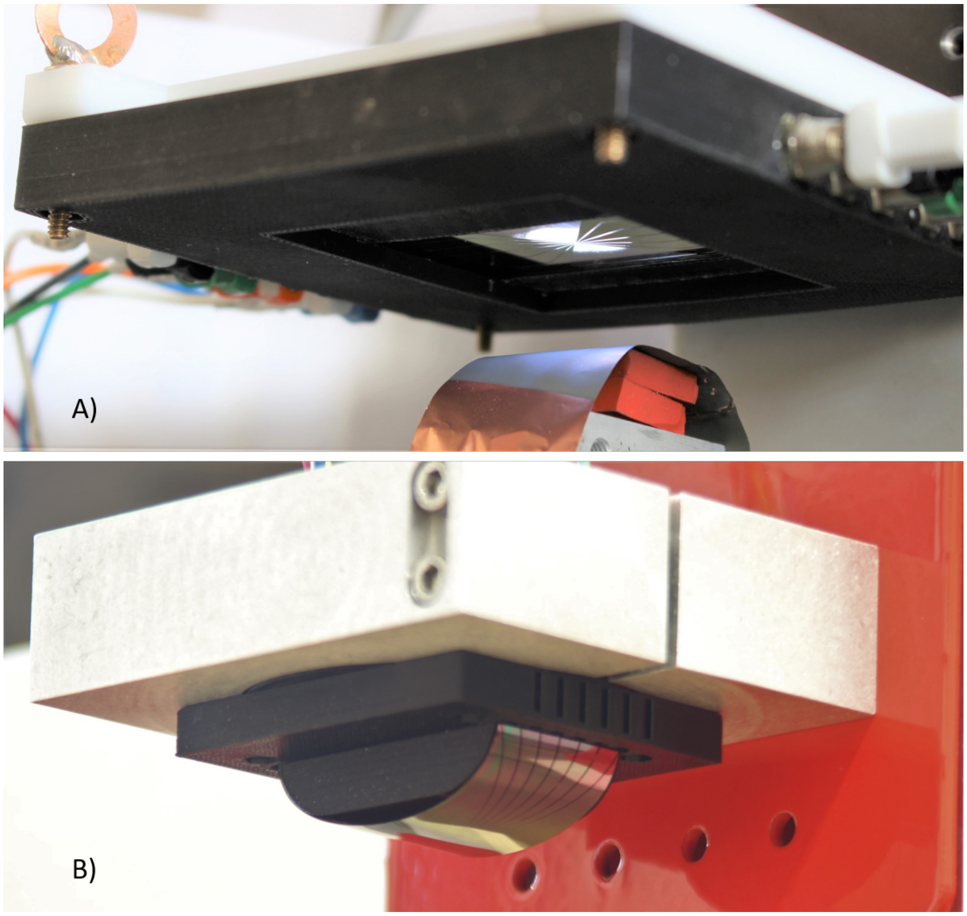

Figure 4.8: Comparison of the custom μNLP (A) and μFLP (B) holders attached to their respective stage mounts. The μFLP holder is not confined to a certain sample area due to no wall constraints.

4.4.3 Development of the Micro-Flex-Line Probe Data Acquisition Circuit

When compared to Figure 4.1, Figures 4.9 and 4.10 below show the two differences between the data acquisition circuits for the μNLP apparatus and the μFLP apparatus. The first difference is the replacement of the Power Supply and Digital Multimeters with Analog Discovery data acquisition modules (ADs). The second change is the addition of a Current Measuring circuit used to calculate I_{in}. Both these modifications are further explained below.

Roles of Analog Discovery 1 and 2

The data acquisition circuit can potentially add a lot of cost and time spent on development due to the the expense of high-end Digital Multimeters that are complicated to setup. Each high-

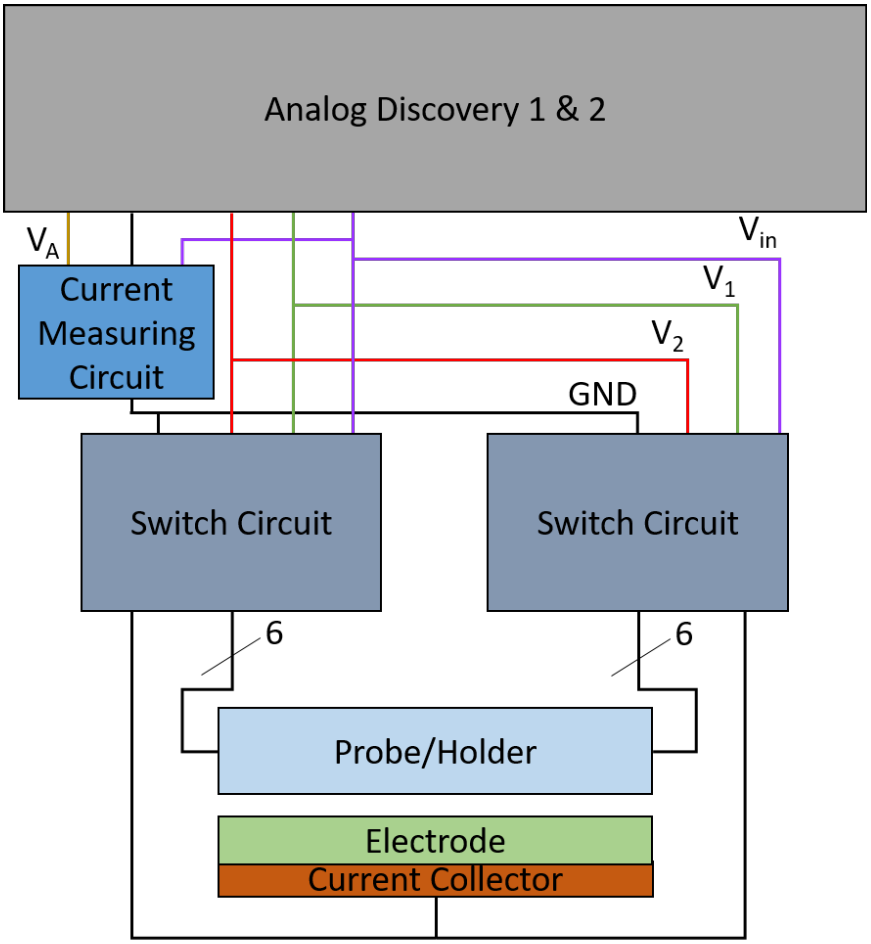

Figure 4.9: Data acquisition schematic for the μFLP measurement apparatus. Data acquired from the probe is measured and stored in a computer by the Analog Discoverys.

accuracy multimeter can cost upwards of $800 and takes time and knowledge of the multimeters software to configure each one to perform the individual tasks of measuring V_{in}, I_{in}, V_1, and V_2 at the appropriate times. To make this section of the new data acquisition circuit develop faster and cheaper, two ADs were purchased from Digilent for about $260 each, see Figure 4.10.

The two ADs (AD_1 and AD_2) can fit in the palm of your hand and replace the functions of all four of the Agilent 34450A Digital Multimeters used in the data acquisition circuit for the μNLP measurement apparatus. This cuts down on cost and drastically increases the portability and user friendliness of the entire apparatus. The ADs connect to the computer via USB connection and are compatible with MATLAB software, allowing them to be controlled easily by the master MATLAB code.

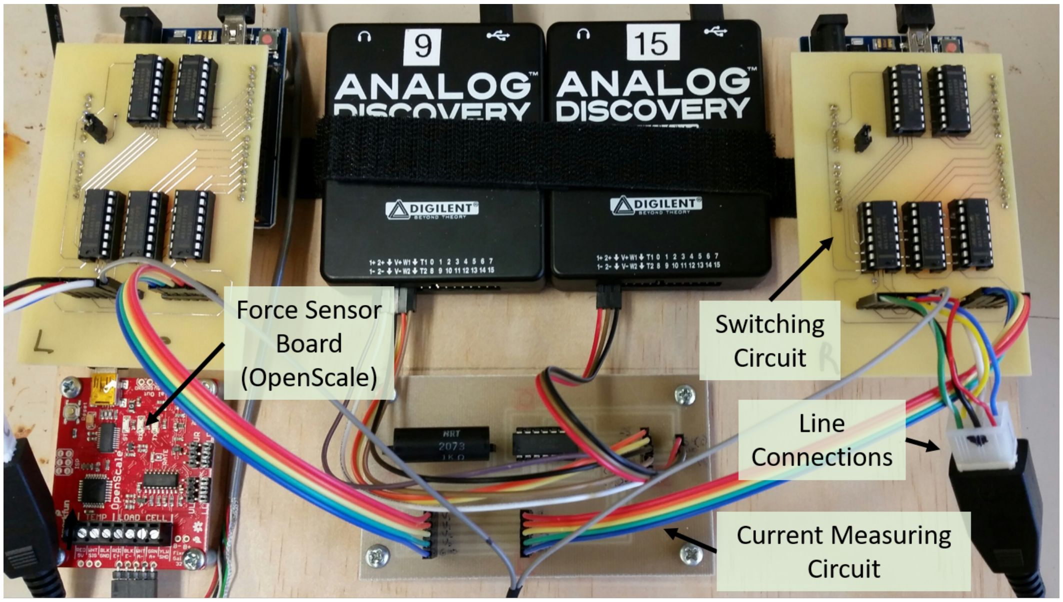

Figure 4.10: Physical circuit of the data acquisition schematic for the μFLP measurement apparatus seen in Figure 4.9.

Table 4.1 explains the individual functions that AD_1 and AD_2 perform, and by which feature of the AD that the function is performed. Only a small fraction of the features available on the AD are being utilized in the data acquisition circuit. The Analog Discovery Technical Reference Manual [29], found on the Digilent web page, further describes its capabilities in detail.

Table 4.1: Individual tasks of Analog Discovery 1 and 2.

AD	**Function**	**Feature Used**
AD_1	Read V_1	Scope Channel 1 Positive
	Read V_2	Scope Channel 2 Positive
	Generate +5 V	±5VDC Power Supply
	Generate -5 V	±5VDC Power Supply
AD_2	Read V_{in}	Scope Channel 1 Positive
	Read V_m	Scope Channel 2 Positive
	Generate V_{in}	Waveform Generator
	Common Ground	Ground

Integration of a Current Measuring Circuit

To calculate the resistance of the electrode volume ($R_{Electrode}$) being sampled, Equation 4.1 must be used. In order to make this calculation, I_{in} must be calculated first. A current measuring circuit is needed to calculate I_{in} because the AD does not have an internal amp-meter. To accomplish this, a simple transimpedance amplifier, as seen in Figure 4.11, was added to the data acquisition circuit.

$$R_{Electrode} = \frac{|V_1 - V_2|}{I_{in}} \tag{4.1}$$

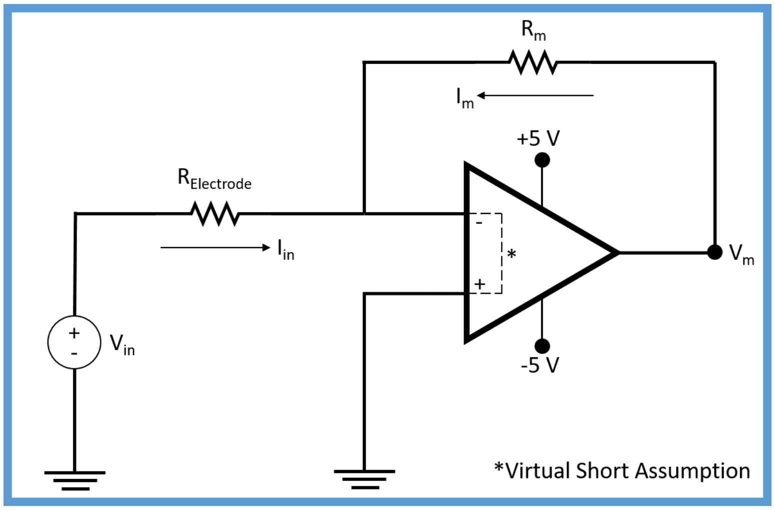

Figure 4.11: Circuit representation of the current measuring circuit block seen in Figure 4.9 and physical circuit pointed to in Figure 4.10.

Equations 4.2 and 4.3 are used to make the I_{in} calculation. R_m is a known value and V_m is measured with one of the scope channel inputs on AD2. The reason why these equations can be applied is because of the virtual short assumption in op-amps. Essentially, meaning that the positive and negative terminals of the op-amp are shorted together and both tied to ground.

$$I_m = \frac{-V_m}{R_m} \tag{4.2}$$

$$I_{in} = |I_m| \tag{4.3}$$

4.4.4 Development of the Micro-Flex-Line Force Sensor Circuit

The signal interpretation hardware used for the force sensor in the μNLP measurement apparatus is extremely accurate, but expensive and they are also complicated to install and use. The NI 9237 4-channel Module alone costs $1354 and it can't be used without the NI 9171 CompactDAQ USB Chassis, which is an additional $308. Furthermore, the NI hardware can only be controlled by LabVIEW software, which needs to be linked to our master MATLAB code. In an effort to make the new μFLP measurement apparatus affordable and compact, new hardware was researched and tested to interpret the signals coming from the force sensor.

After researching different ideas to use various load sensors or build our own scale using strain gauges in a Wheatstone bridge configuration, we decided to make the force measurements from the two different measurement apparatus as similar as possible by using the MLP-100 in the μFLP force sensor circuit as well. The changes made to the force sensor circuit are found in the signal interpretation hardware and software. Instead of having to purchase and use the NI device described above, the SparkFun OpenScale board is used. This little red board is found in the top left corner of Figure 4.6 or closer up in the bottom left corner of Figure 4.10. It replaces the functionality of both the NI devices and cost just under $30. The OpenScale reads and interprets the signals coming from the force sensor and relays this information to the master MATLAB code using Arduino code that is easy to integrate.

4.5 Conclusion

Both the μNLP measurement apparatus and the μFLP measurement apparatus have the same basic function to measure and record data taken with their respective probes. Both apparatus have been tested and found to accomplish this function. In order to do so, the μNLP measurement apparatus has had modifications and improvements to each of the four components of the measurement apparatus described at the beginning of this chapter and the μFLP measurement apparatus was created. Table 4.2 shows the prices of the sub-components in each of the measurement apparatus. The developments and assembly of the new μFLP measurement apparatus show that it can be built for an affordable price and stored in a compact fashion. Having two apparatus to perform measurements with will parallelize the data acquisition and make the gathering of conductivity measurements faster and more efficient.

Table 4.2: Approximate prices of the sub-components in each of the measurement apparatuses.

Apparatus Component	**μNLP Apparatus Prices**	**μFLP Apparatus Prices**
Three-Axis Stage	Newmark Systems XYZ Stage: ∼\$20,000	Shapeoko CNC Stage: \$999.95
Probe Holder	3D Printed Holder: ∼\$20 Accfly Pen Microscope: \$36.99	3D Printed Holder: ∼\$35
Data Acquisition Circuit	Agilent 34450A DAQ: \$827 Agilent 34450A DAQ: \$827 Agilent 34450A DAQ: \$827 Agilent 34450A DAQ: \$827 PS280 DC Power Supply: \$159.99	Analog Discovery: \$259 Analog Discovery: \$259
Force Sensor Circuit	MLP-100 Force Sensor: \$310 NI 9237 Module: \$1,354 NI 9171 Chassis: \$308	MLP-100 Force Sensor: \$310 SparkFun OpenScale: \$29.95
	Total: \$25,496.98	**Total: \$1,892.90**

CHAPTER 5. RESULTS AND DISCUSSION

5.1 Introduction

The first half of this chapter focuses on how electrode samples are tested. The second focuses on the results and validation of tests taken with the μFLP. It is shown that the μFLP takes reliable data and can measure micron-scale variability in the electronic conductivity of electrodes.

5.2 Testing Electrodes

To map the conductivity of a Li-ion electrode, certain parameters need to be taken into account. Two things that have to be known beforehand are how big of an area needs to be tested, and how high of resolution is needed in the map. When the probe and electrode are both mounted, these parameters can be put into the user interface that the master MATLAB code uses. Depending on the dimensions of the test area and the resolution needed in the map, the stage will be commanded to move the probe in a raster pattern, taking tangential and orthogonal measurements at each location (Figure 5.1).

Each location is repeatedly measured 10–20 times, depending on the experiment. When a measurement is “repeated”, this means that the probe moves up in the Z-axis to break all contact with electrode, then moves back down to repeat the measurement. The probe does not move from its X and Y locations, until all the measurements are repeated at the current location. Repeating measurements allows for a mean value to be calculated for that location.

After the testing at each location is finished, the data is stored in an Excel spreadsheet. When the measurement apparatus is finished and the entire specified area is measured, the data can be analyzed by the inversion software discussed by Flygare et al. [17]. The code flags any data that is more than five standard deviations away from the mean or data that is negative. The flagged data is interpreted as a bad data point and thrown out of the final calculation. Poor contact between the lines and the electrode is one cause to collecting a bad data point. Once the data is filtered by this quality criteria, a conductivity value is calculated for each location.

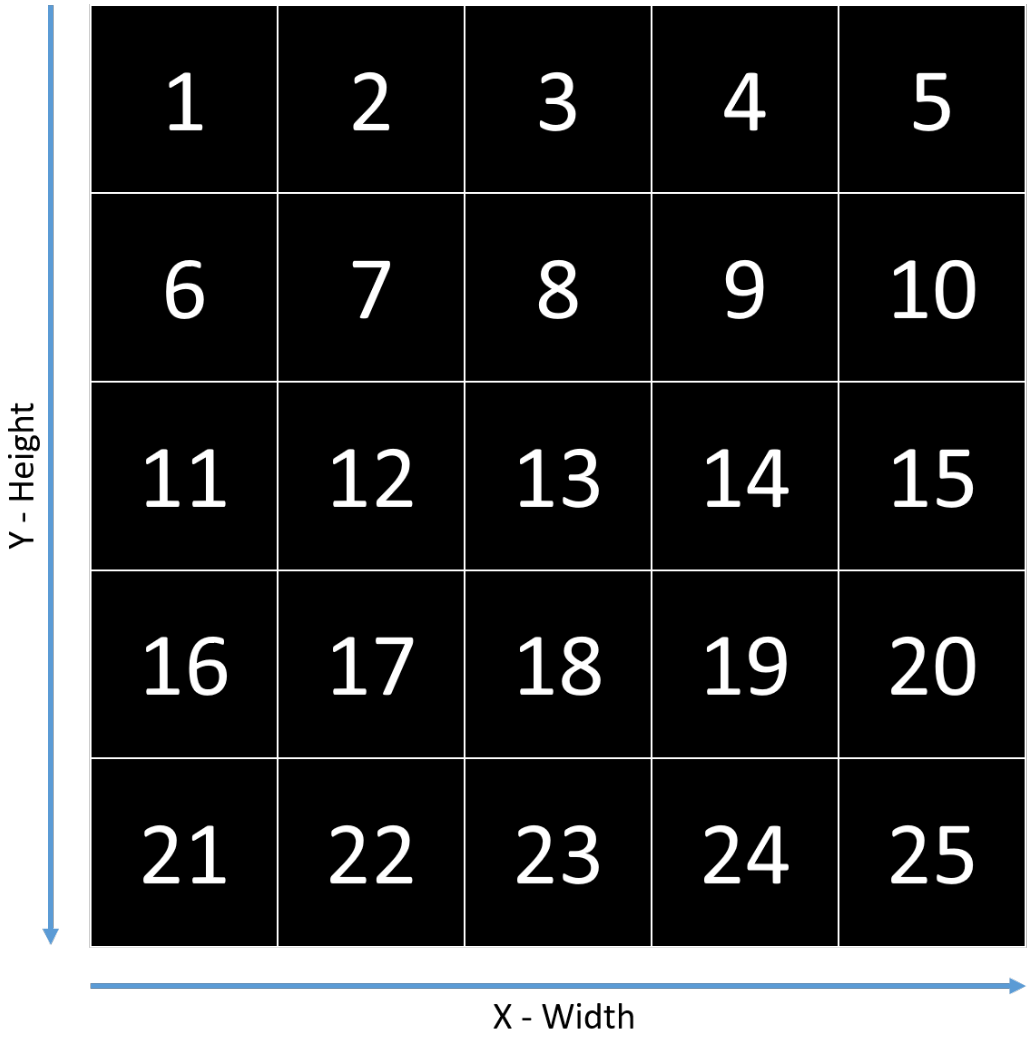

Figure 5.1: The probe will take data in locations 1 through n in a raster path, where n is the number of points specified. This figure is an example of the path the probe would take if the test area were square with 25 points specified.

5.3 Validation and Results

5.3.1 Average Bulk Conductivity

All the commercial-quality samples tested for the purposes of this thesis were graciously donated by Argonne National Laboratory (ANL). The two cathode samples and single anode sample provided are labeled AC005, AC015, and AA002. The first A stands for Argonne, while the following C or A respectively stand for cathode or anode.

To validate the μFLP, the testing procedure outlined in the previous section was performed on all three of the electrodes from ANL, two of which have already been tested by the μ4LP for comparison purposes. There are no results from the μ4LP for the cathode AC015 because it was acquired after the initial testing was performed by Lanterman et al. [12]. This means that both AC005 and AA002 were tests by a μ4LP and a μFLP. It is good to compare results from both anodes and cathodes due to the drastic change in conductivity that is possible between the two types of electrodes.

The sample area consists of 25 points spanning a 2 mm × 2 mm square. Each location is repeatedly measured 15 times to determine a mean conductivity value. All 25 points are then averaged together to find a bulk average conductivity (σ). The results of these tests are found in Table 5.1. The table compares the results calculated with the μFLP to those of the μ4LP previously documented.

Table 5.1: Comparison of the average bulk conductivity of three commercial-quality electrodes provided by Argonne National Laboratory. The average bulk conductivity was calculated from data collected by both the μFLP and the μ4LP in order to validate the μFLP.

Sample	**Method**	**σ(mS/cm)**
AC005	μFLP	241.4±14.6
	μ4LP	201±37
AC015	μFLP	198.2±5.4
	μ4LP	N/A
AA002	μFLP	3961.7±680.7
	μ4LP	4009.8±844.9

From the data provided in Table 5.1, it is seen that the σ calculated from the data collected by both the μFLP and μ4LP are very similar to each other. The slight variation between the values could be caused by anything from a change in sample location, to the amount of time the electrode has been exposed to air between validation measurements. The number following the $\pm$ is the 95% confidence interval. Note that the confidence interval for the μFLP is smaller than the confidence interval for the μ4LP.

Even when using lines instead of points to get better contact with the electrode, it was found that there were still times when the μ4LP and μNLP couldn't make contact on each line. This is possibly due to the 3–5 μm variation in surface roughness on the thin film battery electrodes. Glass cannot conform to accommodate the surface roughness, but the Kapton polyimide substrate of the μFLP provides for a strong device that can conform to the surface that is being tested. This helps each of the six lines to more reliably make sufficient contact with the electrode surface. It has been shown that the flexible probe consistently takes more reliable data than either the μ4LP or μNLP. It is for this reason, we think that the 95% confidence is so much lower for the data taken with the μFLP.

It is interesting to note that the σ for AA002 is almost 20 times larger that that of either AC005 or AC015. Each of the electrodes provided from ANL are made from different mixtures of carbon binding and active material. This being said, it is common to find that the average conductivity of anodes are magnitudes greater than that of a cathode. This is due to the fact that most anodes are graphite-based, and thus are very conductive. This can be seen in Table 5.1 where the average conductivity for AA002 is about 4000 mS/cm, and the average conductivity for both AC005 and AC015 are close to 200 mS/cm.

5.3.2 Mapping Conductivity

Finding the average bulk conductivity is useful for validation and comparing probes or electrodes to one another, but to truly see variation of conductivity in thin-film electrodes on a micron-scale, a map of the sample area needs to be constructed. When all the data is filtered and the conductivity values are found for each point, they are inserted into a contour plot to create a conductivity map like those found in Figures 5.2 and 5.3. The map is color coordinated to make viewing it as intuitive as possible. Light yellow and dark blue areas on the map each respectively signify hot spots or cold spots in conductivity. The color scale changes relative to the electrode being tested, due to each electrode having a different ranges of local conductivity. The plots below each of the respective conductivity maps in figures 5.2 and 5.3 show the conductivity values for each of the 25 points in the measurement area. Refer to Figure 5.1 for the testing order that the probe takes.

The conductivity maps and respective plots were constructed from the same data collected to make Table 5.1. Both of the samples (AC005 and AC015) are cathodes, meaning it is expected to see lower conductivity. Furthermore, we can expect to find the average conductivity and variations in conductivity to be on the same magnitude, which they are. It is seen that there is relatively large variation in conductivity in both of the cathode sample areas.

The 95% confidence uncertainty for the μFLP measurements seen in Table 5.1, in general, are less than the variation seen from one location to another on the sample area. This indicates that the seemingly anomalous hot and cold spots are due to a material difference at that locations. This shows that the average bulk conductivity of thin-film electrodes is non-homogeneous even on a millimeter-scale. This non-homogeneity is seen in the two cathodes tested above by the 100–140 mS/cm variation in conductivity across the 2 mm × 2 mm area.

5.4 Summary

The μFLP is able to measure location variability in the electronic conductivity of electrodes on a millimeter and even micrometer scale. By repeatably sampling the conductivity values over multiple locations, a reliable average bulk conductivity of the electrode samples can be estimated. By plotting the conductivity data in a contour map, the change in bulk conductivity can visibly be tracked as it changes from one location to another.

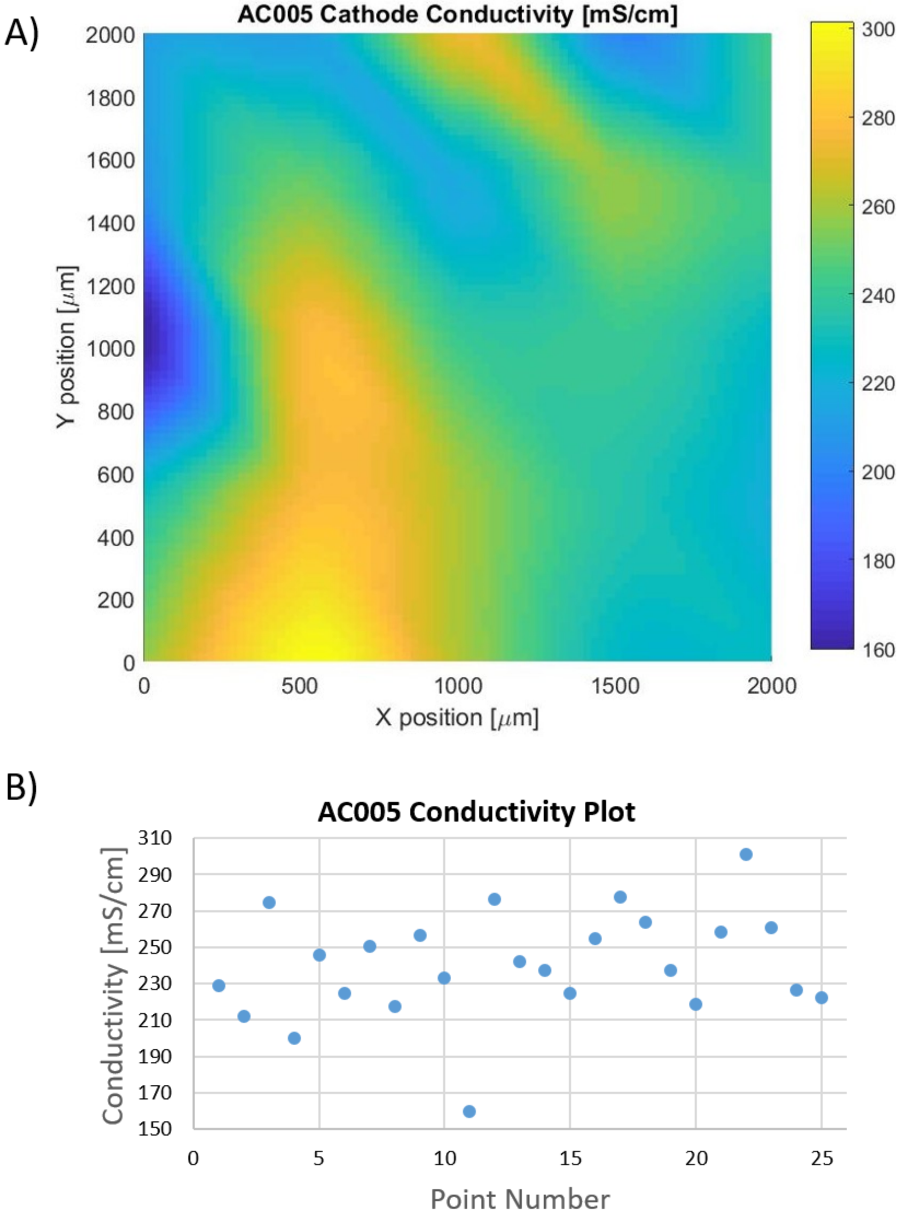

Figure 5.2: Conductivity map (A) and plot (B) of Argonne National Laboratory cathode sample AC005. There is a 140 mS/cm variation in conductivity shown in the 2 mm × 2mm area of the electrode.

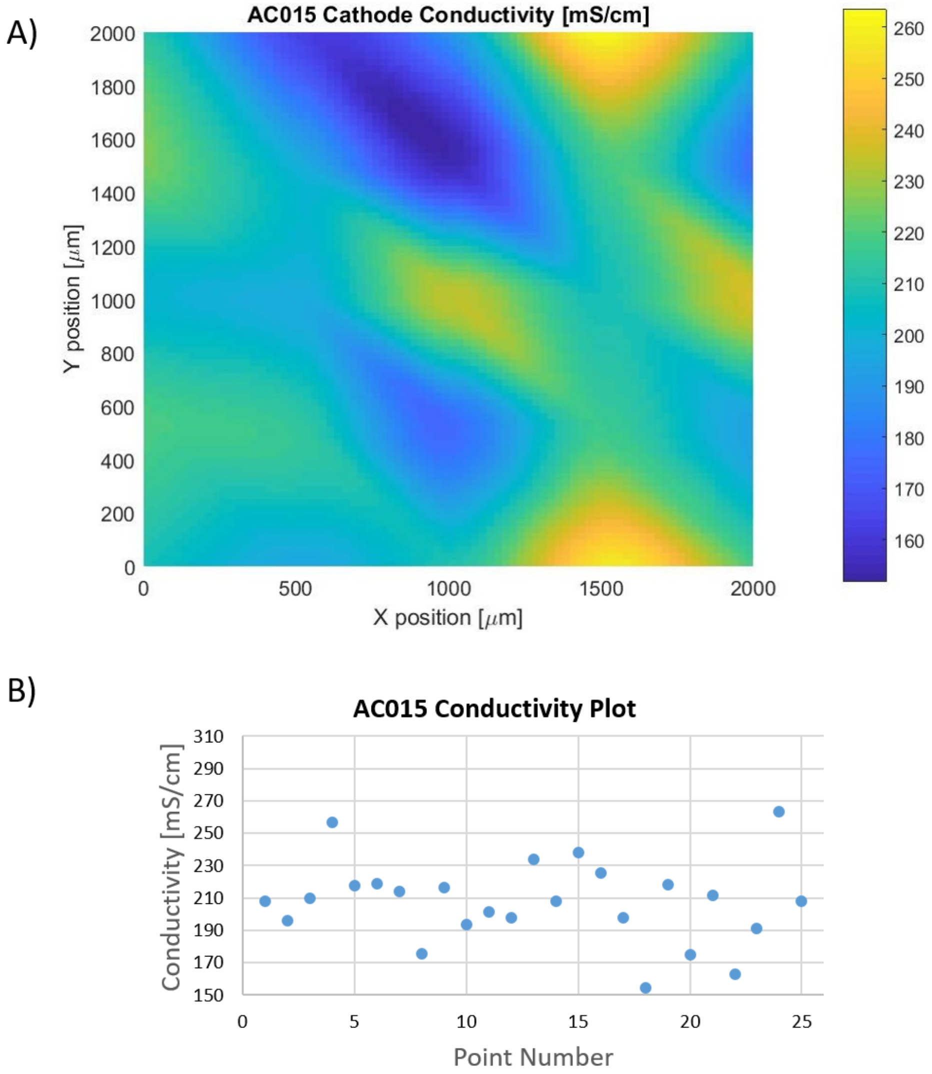

Figure 5.3: Conductivity map (A) and plot (B) of Argonne National Laboratory cathode sample AC015. There is a 100 mS/cm variation in conductivity shown in the 2 mm × 2mm area of the electrode.

CHAPTER 6. CONCLUSION

This chapter contains a summary of the accomplishments and conclusions of this project. It also outlines the contributions the project has made to the fields of thin-film electrodes and microfabrication of flexible circuits. Finally, it contains topics for which areas of future work can be applied to the project in order to improve our probes.

6.1 Experimental Conclusions

Fabrication of working μNLPs and μFLPs was successful in that the probes were made to the specific design parameters outlined in Chapter 3. To collect experimental data from the probes, a previously used measurement apparatus was improved and another was developed (see Chapter 4) to house and maneuver each device respectively. The measurement apparatus constructed for the μFLP is sufficient to reach the same capabilities of the more expensive apparatus used for the μNLP, but for a fraction of the price and size. Together, the probe and apparatus are used to take measurements of thin-film battery electrodes. The data collected is analyzed to construct conductivity maps of the tested electrodes.

The μFLP can accurately and non-destructively measure the local conductivity of thin-film battery electrodes. It has been validated by comparing measurement results of various commercial grade, thin-film electrodes to those of the previously validated μ4LP through use of the van der Pauw method [30]. These results prove that the μFLP receives similar results to μNLP. From this, we know that the mathematical model used to invert the date generated from the probe is working correctly. The results provided by the μFLP can be displayed in easy-to-read maps of conductivity that can be used to identify hot or cold conductivity locations on the electrode.

6.2 Contributions to Fields of Research

This project, though focused on the battery materials research, impacts more than just the field of thin-film electrodes. The implementation of a working flexible device (μFLP) shows that the research conducted through this project impacts the field of flexible circuits as well. The merging of these two fields of study form a field that is uniquely suited for improving the manufacturing of thin-film electrodes and ultimately achieve our goal to improve the lifetime and durability of thin-film batteries.

Initial tests taken with the μFLP show that it can be invaluable to test the conductivity of electrodes during the actual fabrication process of thin-films. As seen in Chapter 4, the custom probe holder designed to house the μFLP is rounded to mimic the probe being mounted onto a cylindrical roller. Successful tests with this holder form a proof of concept that the μFLP can be used in a production line by mounting it onto a wheel that would periodically take measurements as the film passes underneath it.

6.3 Future Research Areas

6.3.1 Smaller Probe Window Dimensions

In Chapter 3, the dimensions of the contact lines are described to create a window of 250 μm $\times$ 220 μm. These dimensions were chosen for reasons related to making the fabrication and testing each respectively easier and more intuitive. This window size is acceptable for taking measurements with our probes, but to improve the accuracy of the data and increase the resolution of the conductivity maps, the project should move to a smaller, square window.

I propose the window dimensions to be 110 μm $\times$ 110 μm. This would make the six contact lines on the μFLP each 10 μm wide with 10 μm spacing. Although fabrication will become slightly harder due to smaller features, two aspects of the data collection will be improved through this change:

- Resolution of the conductivity maps will be quadrupled because the perimeter of the window is roughly halved. Being able to take measurements closer together will help narrow down reasons why hot spots and cold spots in conductivity occur.

- Shunt current passing through the current collector during tangential measurements will be reduced due to the path between V_{in} and Ground being shortened by half. This will reduce our margin of error caused by the mathematical model having to account for the less shunt current.

6.3.2 Gold Plating

After the electrodeposition of copper onto the nickel lines, as described at the end of Chapter 3, the copper lines should be coated in a thin layer of gold. This would add a small amount of time onto the fabrication process, but it would improve the robustness of the lines. Coating the copper lines in gold would give them the strength of nickel and copper, and the conductivity and corrosion resistance of gold.

6.3.3 Jail-Bar Design

After many hundreds of test measurements, the probe can sometimes fail due to pieces of carbon binder and active material from the electrode packing into the spaces between the lines. This can either short the lines together or even break them off entirely. This problem could be fixed by adding a so called "Jail-Bar" design into the probe fabrication steps. The change would have to be made to the photolithography mask seen in Figure 3.7. The jail-bar design would fill the spaces between the lines with SU-8 to help support them and reduce the risk of packing carbon binder and active material between them. Compare Figure 6.1 below to the last step in Figure 3.6 to see the difference in the window that the jail-bar design would make.

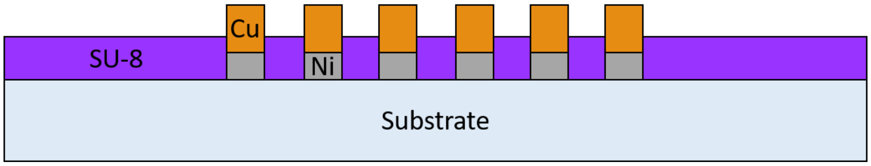

Figure 6.1: Layer profile of the "Jail-Bar" design. SU-8 is found between each of the lines to protect and support them.

6.3.4 Outsourcing Fabrication of the Micro-Flex-Line Probe

A goal that the project should strive to reach is the ability to make the μFLP in large-scale quantities. When the design and fabrication details of the μFLP stabilize, I propose that the fabrication of the probe be outsourced to a third party company that has the means to mass produce our probe. This would allow the project to focus on analyzing conductivity data gathered from testing thin-film battery electrodes.

Bibliography

[1] MarketWatch, "Lithium-ion Battery Market is Projected to Reach US $77.42 bn in 2024; Global Industry Analysis, Size, Share, Growth, Trends and Forecast 2016 - 2024: TMR." PR Newswire Europe, Sep 2016. 1

[2] Statista, "Projected Split of The Global Lithium-ion Battery Market in 2020, by Segment." `https://www.statista.com/statistics/309579/lithium-ion-battery-market-estimation`, 2017. 1

[3] I. Buchmann, "BU-205: Types of Lithium-Ion." `http://batteryuniversity.com/learn/article/types_of_lithium_ion`, Nov 2016. 1

[4] L. Valoen and M. Shoesmith, "The Effect of PHEV and HEV Duty Cycles on Battery and Battery Pack Performance," in *PHEV 2007 Conference*, (E-One Moli Energy (Canada) Ltd., 20,000 Stewart Crescent, Maple Ridge, BC,), 2007. 1

[5] Acquire Media, *Tesla Q4 2016 Production and Deliveries*, Jan 2017. 2

[6] U.S. Cencus Bureau, *U.S. and World Population Clock*, jan 2017. 2

[7] A. Smith, "U.S. Smartphone Use in 2015," internet, science, and tech, Pew Research Center, 2015. 2

[8] J. Mouawad, "Report on Boeing 787 Dreamliner Battery Flaws Finds Lapses at Multiple Points," *The New York Times*, 2014. 3

[9] Samsung, "[Infographic] Galaxy Note7: What We Discovered." `https://news.samsung.com/global/infographic-galaxy-note7-what-we-discovered`, jan 2017. 3

[10] M. Park, X. Zhang, M. Chung, G. Less, and A. Sastry, "A review of conduction phenomena in Li-ion batteries," *Journal of Power Sources*, vol. 195, pp. 7904–7929, Dec 2010. 3

[11] R. Dominko, M. Gaberscek, J. Drofenik, M. Bele, and S. Pejovnik, "A Novel Coating Technology for Preparation of Cathodes in Li-ion Batteries," *Electrochemical and Solid-State Letters*, vol. 4, no. 11, pp. A187–A190, 2001. 5

[12] B. Lanterman, A. Riet, N. Gates, J. Flygare, A. Cutler, J. Vogel, D. Wheeler, and B. Mazzeo, "Micro-four-line Probe to Measure Electronic Conductivity and Contact Resistance of Thin-Film Battery Electrodes," *Journal of The Electrochemical Society*, vol. 162, no. 10, pp. A2145–A2151, 2015. 5, 6, 8, 9, 10, 11, 54

[13] S. Ramdon and B. Bhushan, "High resolution morphology and electrical characterization of aged Li-ion battery cathode," *Journal of Colloid and Interface Science*, vol. 380, no. 1, pp. 187–191, 2012. 5

[14] M. Kerlau, M. Marcinek, V. Srinivasan, and R. Kostecki, "Reprint of 'Studies of local degradation phenomena in composite cathodes for lithium-ion batteries'," *Electrochimica Acta*, vol. 53, no. 3, pp. 1385–1392, 2007. 5

[15] F. Smits, "Measurement of sheet resistivities with the four-point probe," *The Bell Systems Technical Journal*, vol. 37, no. 3, pp. 711–718, 1958. 5

[16] E. Perkins, L. Barreto, J. Wells, and P. Hofman, "Surface-sensitive conductivity measurement using a micro multi-point probe approach," *Review of Scientific Instruments*, vol. 84, no. 3, 2013. 5

[17] J. Flygare, A. Riet, B. Mazzeo, and D. Wheeler, "Mathematical Model of Four-Line Probe to Determine Conductive Properties of Thin-Film Battery Electrodes," *Journal of The Electrochemical Society*, vol. 162, no. 10, pp. A2136–A2144, 2015. 6, 8, 10, 38, 52

[18] S. Peterson and D. Wheeler, "Direct Measurements of Effective Electronic Transport in Porous Li-ion Electrodes," *Journal of The Electrochemical Society*, vol. 161, pp. A2175–A2181, jul 2014. 7

[19] IMMERSE, "Welcome to the BYU Cleanroom - The Integrated Microfabrication Lab." `http://www.cleanroom.byu.edu`, 2017. 17

[20] H. Lorenz, M. Despont, N. Fahrni, N. LaBianca, P. Renaud, and P. Vettiger, "SU-8: a low-cost negative resist for MEMS," *Journal of Micromechanics and Microengineering*, vol. 7, no. 3, 1997. 21

[21] DuPont, "DuPont Kapton General Specifications." `http://www.dupont.com/content/dam/dupont/products-and-services/membranes-and-films/polyimde-films/documents/DEC-Kapton-general-specs.pdf`, 2012. 24, 27

[22] DuPont, "General Information." `http://www.dupont.com/content/dam/dupont/products-and-services/membranes-and-films/polyimde-films/documents/DEC-Kapton-summary-of-properties.pdf`, 2012. 24, 26, 27, 28

[23] D. Miles, *Polymer Technology*, ch. 17. Chemical Publishing Co., 3rd ed., 1996. 24, 27

[24] V. Ratta, *Crystallization, Morphology, Thermal Stability and Adhesive Properties of Novel High Performance Semicrystalline Polyimides*. Dissertation, Virginia Tech, 1999. 25

[25] A. McNaught, *The Gold Book*. Blackwell Scientific Publications, 2nd ed., 1997. 25

[26] N. Greeves, "Kapton (Polyimide)." `http://www.chemtube3d.com/polymer/_KaptonF.html`, 2008. 25

[27] M. Ghosh, *Polyimides: Fundamentals and Applications*, ch. 1. CRC Press, 1996. 25

[28] M. Tan, C. Guymon, D. Wheeler, and J. Harb, "The Role of SPS, MPSA, and Chloride in Additive Systems for Copper Electrodeposition," *Journal of The Electrochemical Society*, vol. 154, no. 2, pp. D78–D81, 2007. 31

[29] Digilent, *Analog Discovery Technical Reference Manual*, 2017. 48

[30] L. J. van der Pauw, “A method of measuring specific resistivity and Hall effect of discs of arbitrary shape,” *Philips Research Reports*, vol. 13, no. 1, pp. 1–9, 1958. 59

APPENDIX A. PROBE FABRICATION STEPS

The probe fabrication recipe found below is a step by step list of all the procedure performed in order to make our probes. Steps with the sub-label (a) refer to the μNLP, while steps with the sub-label (b) refer to the μFLP. See Figure 3.6 for a visual representation of the recipe steps.

1-a. Clean and Prepare 4 in SiO_2 Wafer for Nickel Deposition

   a. Dip wafer in HF for 30 seconds.
   b. Rinse wafer off thoroughly with DI water.
   c. Put wafer in dry oven for 20 min set at 150 °C.
   d. Plasma descum the wafer for 45 seconds using Plasma Etcher.

1-b. Clean and Prepare 4 in Kapton Wafer for Nickel Deposition

   a. Cut Kapton sheet to fit a mounting wafer.
   b. Mount Kapton to wafer.
      i. Cut parafilm to fit mounting wafer.
      ii. Place cut parafilm on the wafer.
      iii. Set wafer on a hot plate at 90 °C for 10 seconds to melt the parafilm to the wafer.
      iv. Remove wafer from hot plate and roll Kapton onto parafilm to reduce air bubbles.
      v. Set wafer on a hot plate at 90 °C for 10 seconds to melt the parafilm to the wafer and Kapton.
   c. Place the wafer on the cleaning spinner and spin off Acetone and IPA.

2. Deposit Nickel onto Wafer

   a. Use the E-Beam Evaporator to deposit about 190 nm of Nickel onto the wafer.

3. Apply and Develop AZ3330
   a. Place 5-7 drops of HMDS onto the wafer.
   b. Spin at 1000 RPM for 10 seconds.
   c. Place a half-dollar sized amount of AZ3330 onto the center of wafer.
   d. Spin on AZ3330 using 3 step program:
      i. 500 RPM for 5 seconds
      ii. 3000 RPM for 60 seconds
      iii. 6000 RPM for 2 seconds
   e. Soft-bake on hot plate for 60 seconds at 90 °C.
   f. Place in aligner, apply mask, and expose for 14 seconds.
   g. Develop for 45 seconds in 300 MIF.
   h. Hard-bake on hot plate for 60 seconds at 110 °C.
4. Etch Nickel and Remove AZ3330
   a. Place wafer in Nickel Etchant at room temperature and wait 2-5 minutes depending on thickness, temperature, and stirring for nickel to etch.
   b. Rinse thoroughly with DI water and dry both side completely.
   c. Place wafer on spinner and strip off the AZ3330 with Acetone and IPA.
   d. Place wafer in oven for 20 min at 150 °C.
5. Apply and Develop SU-8 2000.5
   a. Place 5-7 drops of HMDS onto the wafer.
   b. Spin at 1000 RPM for 10 seconds.
   c. Place a half-dollar sized amount of SU-8 onto the center of wafer.
   d. Spin on SU-8 using 3 step program:

        i. 500 RPM for 5 seconds
        ii. 1000 RPM for 60 seconds
        iii. 6000 RPM for 2 seconds
    e. Soft-bake on hot plate:
        i. 60 seconds at 65 °C
        ii. Set to 95 °C and wait 3 min
        iii. Let hot plate cool back down to 65 °C
    f. Place in aligner, apply SU-8 mask 1, and expose for 30 seconds.
    g. Post exposure bake on hot plate:
        i. 60 seconds at 65 °C
        ii. Set to 95 °C and wait 4 min
        iii. Let hot plate cool back down to 65 °C
    h. Develop wafer in SU-8 Developer for about 50 seconds.

6. Apply and Develop SU-8 20005
    a. Place 5-7 drops of HMDS onto the wafer.
    b. Spin at 1000 RPM for 10 seconds.
    c. Place a half-dollar sized amount of SU-8 onto the center of wafer.
    d. Spin on SU-8 using 3 step program:
        i. 500 RPM for 5 seconds
        ii. 3000 RPM for 60 seconds
        iii. 6000 RPM for 2 seconds
    e. Soft-bake on hot plate:
        i. 60 seconds at 65 °C
        ii. Set to 95 °C and wait 3 min
        iii. Let hot plate cool back down to 65 °C

f. Place in aligner, apply SU-8 mask 2, and expose for 30 seconds.

g. Post exposure bake on hot plate:

   i. 60 seconds at 65 °C

   ii. Set to 95 °C and wait 4 min

   iii. Let hot plate cool back down to 65 °C

h. Develop wafer in SU-8 Developer for about 2 min.

7-a. Dice SiO_2 Wafer to Size

a. Using a dicing saw, cut the wafer to the probe dimensions.

7-b. Dismount Kapton Wafer and Cut to Size

a. Put a couple drops of Acetone in between the Kapton and Parafilm and gently peal away the Kapton wafer.

b. Using scissors, cut the Kapton to the probe dimensions.

8. Electroplate Up Probe Lines

a. Insert probe into electroplating stage

b. Electroplate copper onto the lines using copper solution until the lines are about 1–2 μm above the SU-8 layer.

c. Clean probe using DI water.

d. Electroplate thin layer of gold onto the the lines.

e. Clean probe using DI water.